NTNU – Trondheim
Norwegian University of
Science and Technology

Protein Binding and Crowding Effects on DNA Condensation

Petter Langlete

Master of Science in Physics and Mathematics
Submission date: June 2015
Supervisor: Rita de Sousa Dias, IFY

Norwegian University of Science and Technology
Department of Physics

Abstract

The main goal of this work is to map how bacterial nucleoid associated proteins (NAPs) condense DNA in tandem with a crowded environment, since this may provide useful information for research where DNA compaction and protein binding is of high importance, such as protein expression, gene therapy and cancer research. The isolated effects of NAPs on condensation are subject to constant investigation, but little is known about the combination of both protein binding and crowding effects in vitro. The combined effects of crowding and condensing agents on DNA compaction are investigated with fluorescence spectroscopy (FS), fluorescence correlation spectroscopy (FCS), atomic force microscopy (AFM), cell-free expression assays and electrophoresis mobility shift assays (EMSAs). Plasmid pSB-M2g-1-17 was harvested from DH5-α *Escherichia coli*, and subjected to polyethylene glycol (PEG) and the condensing polyamine spermine. Histone-like nucleoid-structuring protein (H-NS) was over-expressed, purified and its activity confirmed. A 4017 bp amplicon from template plasmid pSB-E1g, including a T7 promoter and a gene encoding green fluorescent protein (GFP), was used to quantify DNA compaction and protein expression under influence of PEG and H-NS. The combined effect of PEG and spermine was found to reduce the hydrodynamic volume of DNA to 5% of its initial value, while spermine and PEG alone reduced it to 33% and 23%, respectively, although with considerable standard deviations. $0.5 \rightarrow 1.0$ μM H-NS was found sufficient to inhibit cell-free expression of GFP, and 5 μM induced visual DNA-aggregation by AFM. Novel insight in synergism was attained, as crowding was shown to greatly reduce the amount of H-NS required for condensation as measured by FCS.

Sammendrag

Målet for dette arbeidet er å kartlegge hvordan bakterielle nukleoid-assosierte proteiner (NAPs) pakker DNA i samarbeid med trengselseffekter, da dette kan føre til nyttig informasjon for forskningsfelt der DNA-kompresjon og proteinbinding er av høy interesse, som proteinsyntese, genterapi og kreftforskning. Det forskes mye på de isolerte effektene av NAPs på DNA-kompresjon, men man vet lite om den kombinerte effekten av både proteinbinding og trengsel in vitro. Denne masteroppgaven omfatter forskning på den kombinerte effekten av DNA-pakkende biomolekyler og molekylær trengsel, ved bruk av fluorescens-korrelasjon-spektroskopi (FCS), fluorescens-spektroskopi (FS), atomkraftmikroskopi (AFM), cellefri proteinsyntese, og elektroforese-mobilitet-skift-analyse (EMSA). Plasmid pSB-M2g-1-17 ble høstet fra DH5-α *Escherichia coli*, og utsatt for polyetylen glykol (PEG) og den DNA-pakkende polyaminen spermin. Histone-like nucleoid-structuring protein (H-NS) ble over-uttrykt, renset og dets aktivitet bekreftet. Et amplikon på 4017 bp som inneholdt en T7-promoter og et gen for grønt fluorescerende protein (GFP) ble oppformert fra plasmidet pSB-E1g og brukt til å kvantifisere DNA-kompresjon og proteinsyntese under påvirkning av PEG og H-NS. Den kombinerte effekten av PEG og spermin ble ansltt til redusere det hydrodynamiske volumet til DNA til 5% av dets opprinnelige størrelse, mens spermin og PEG alene reduserte det til 33% og 23%, respektivt, dog med store feilmarginer. $0.5 \rightarrow 1.0$ μM H-NS var tilstrekkelig for senke cellefri syntese av GFP, og 5 μM førte til observerbar DNA-aggregering ved bruk av AFM. Forskningen førte til ny innsikt i synergiske effekter da molekylær trengsel reduserte den nødvendige mengden H-NS for å oppnå målbar kompresjon i FCS.

Preface

This thesis describes work performed at NTNU autumn 2014 through spring 2015. Parts of the text, mainly what is referred to as *prevoius data*, is a continuation of work already considered in a project assignment submitted December 2014, and is included for comparison. The complete work should equal 30 credits. I would like to express my sincere gratitude for all guidance provided by my laboratory partner Ph.D student Sravani Keerthi Ramisetti, and my supervisor, Associate Professor Rita de Sousa Dias. I would also like to thank Dr. Astrid Bjørkøy and Dr. Sylvie Lelu for invaluable technical support with the fluorescence microscope, and Dr. Rahmi Lale and Dr. Simone Balzer Le for help with cell lines and DNA synthesis.

Contents

List of Figures

Glossary and Abbreviations

ACF	=	Auto-correlation function
AFM	=	Atomic force microscopy
APD	=	Avalanche photo diode
AT-rich	=	Adenine-thymine rich
bp	=	(DNA)- base-pair
BSA	=	Bovine serum albumin
cat.#	=	Catalog number
CLSM	=	Confocal laser scanning microscope
DMSO	=	Dimethyl sulfoxide
EMSA	=	Electrophoresis mobility shift assays
FCS	=	Fluorescence correlation spectroscopy
FS	=	Fluorescence spectroscopy
H-NS	=	Histone-like nucleoid-structuring protein
LaTeX	=	Typesetting software
MQ-water	=	Milli-Q water
PCR	=	Polymerase chain reaction
PEG	=	Polyethylene glycol
SDS	=	Sodium dodecyl sulfate
Spm	=	Spermine
TikZ	=	Graphics Toolbox for LaTeX

Chapter 1

Introduction

1.1 Background

Condensation of DNA is a central effect in countless natural and manufacturing applications, such as gene expression, viral transfection, transformation, therapy and biosensors [1][2][3]. DNA, without some form of compaction, is a fairly large biopolymer, and therefore, evolution has armed all forms of life with numerous strategies enabling DNA to occupy as small a space as possible. These effects have been a matter of ongoing research since the re-statement of Francis Crick's central dogma of molecular biology, the notion that our genetic heritage consists of DNA, which through an RNA transcript translates to our proteome [4]. Furthermore, it is known that the cell decompacts sections of the DNA to make them available for expression mechanisms [5], but the underlying principles are still unclear. This insight in the molecular machinery of DNA dynamics remains a central goal in the field of biophysics, and could yield important applications in medicine and biophysics in general. The research presented in this report is mainly aimed at understanding the underlying principles of DNA compaction and protein binding in bacterial cells, but secondly, it is expected to yield knowledge that can be applied in fields where DNA compaction is of importance, such as non-viral gene therapy and cancer research.

DNA strands occupy only a fraction of their unconstrained volume when in condensed form. For example, the nucleoid space of *Escherichia Coli* has a volume of only 0.5 μm^3, but it contains a genome with an unconstrained volume of 200 μm^3 [6]. The observed condensation is a result of a whole spectrum of synergistic and competitive factors, such as DNA-associated protein, ionic strength, pH, crowding effects and supercoiling [7].

The idea of gene therapy dawned soon after the central dogma of molecular biology [8]. A new or inherited mutation in a gene can lead to changes in the corresponding proteins, with the possibility of detrimental loss of function. An unfortunate combination of such mutations may result in cancer, and depending on cell type and pairing, loss of function can lead to genetic disorders. Some of these, we have no cure for, and only poor treatment

alternatives. The objective of gene therapy is therefore to insert a gene coding for either the functional version of the protein, or a therapeutic drug into the target cell, resulting in restored function or at least satisfactory treatment. Some treatments seek to insert the gene into the germ line, making it inheritable for offspring, while others avoids insertion, and some would even require repeated therapies [9]. In theory, one could genetically modify a patients germ line to stop inheritance of genetic disease, but this is indeed a risky endeavour, due to limited knowledge about the long-term consequences, as well as the complex ethical considerations on the subject [10]. Therefore, mainly somatic treatments with non-integrative vectors are researched [11]. Typical examples of current research are inserting a functional Cystic Fibrosis Transmembrane Regulator gene into the genome of a patient with cystic fibrosis [12], or to extract and transform stem cells from a patients blood to cure thalassemia [13].

The main obstacle in gene therapy is the design of a safe and efficient drug delivery system. Although experiments with naked DNA have shown some effect [14], successfull transfection generally requires a vector [15]. The goal of the vector is to reach a desired number of targeted cells, and deliver a lasting dose of functional genetic material. There are many obstacles for a gene vector, including extra-cellular tissues, cellular membranes and agents of the immune system. The ability for a particle to overcome these obstacles depends strongly on the size, charge and hydrophobicity. It has been shown that the extracellular matrix acts as an electrostatic bandpass filter [16], in which small particles of close to neutral charge, have the greatest diffusive power. In order for a vector to achieve desired size, the residing DNA has to be as compact as possible.

1.2 Project Background

The laboratory investigation presented in this report is a contribution to the research project of Rita de Sousa Dias and Sravani Keerthi Ramisetti, which entails the combined effects of condensing and crowding agents on DNA compaction. Previously, the seemingly synergistic effects of Polyethylene Glycol (PEG) and spermine has been mapped by dye exclusion experiments with fluorescence spectroscopy (FS), thus some work with this method was executed for complementary results. Due to the differing requirements for sample preparation for FS and fluorescence correlation spectroscopy (FCS), standardization of protocols and selection of suiting sample sources consumed more time than expected, but ultimately proved invaluable for effective use of FCS. A reliable FCS investigation of DNA condensation under differing combinations of H-NS, PEG and BSA is the main novel feature of the laboratory investigation, and the data will be featured in a paper, “In vitro studies of single molecule DNA compaction by H-NS protein in the presence of a crowded environment.” (Ramisetty SK, Langlete P, Dias RS.), in 2015.

Chapter 2

Theory

2.1 DNA Condensation

DNA, in its common, double-stranded form, is a negatively charged biopolymer with a relatively high persistence length of about 35-50 nm [17], depending on conformation and solution conditions. The persistence length is defined as the length of which the directions of the ends no longer correlate. If not specified otherwise, the term DNA generally refers to its double-stranded form. This configuration is a key contributor to the observed rigidity, which can be appreciated when compared to single-stranded DNA, which displays only a fraction of the persistence length, about 2 nm [18]. The net negative charge of DNA arises from unpaired electrons of the oxygen in the phosphate backbone, one net negative charge per base, two per base-pair. DNA, therefore, is always surrounded by co-ions, and its behaviour is dictated by the features of these. In cells, many different ions and molecules are present, which affect DNA compaction in some way, some acting synergistically, while others have a competing function [19].

Ionic Strength, pH and Dielectric Constant

The presence of multivalent cations has been shown to lead to the condensation of DNA [20]. Since nucleotides are negative, these positive ions associate to DNA, leading to electrostatic screening, and, depending on valence, can attract and bridge different segments of the polymer. Spermine, used in this work, is a valence +4 polyamine, and was recognized as a condensing agent in early DNA condensation experiments [21]. The structure of spermine is shown in Figure 2.1, where the four amine groups are visible. All of these have high affinity to H^+-ions at physiological pH, resulting in the cationic nature of the molecule. It is found in eukaryotic metabolism [22], and is an essential growth factor in some bacteria [23].

The ionic strength has a variety of effects. As mentioned, electrostatic screening could enable DNA compaction, but high ionic strength could also lower the affinity of polyca-

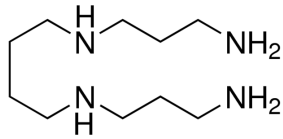

Figure 2.1: General molecular formula of spermine [24].

tions or binding proteins, which then could be required in higher concentrations to induce condensation [25]. The salt conditions of the solvent are very important for the function of some proteins so when constructing a model cytoplasm for investigating protein activity, care must be taken to make simple, but still satisfactory salt conditions for the protein in question to function. For instance, the ionic strength could be the same for a solution of KCl and one of $MgCl_2$, but a protein could have significantly altered activity in absence of divalent ions, making the KCl inadequate as the only salt [26].

As with cation presence, the pH will effect the condensation of DNA. Considering the naked DNA, an increase in H^+ will shield charges on the backbone and shorten persistence length. However, the case is not as straight forward with condensing factors present. For example, it has been shown that increase in pH will increase the persistence length of oxaliplation-condensed DNA [27], while it will reduce the hydrodynamic radius of spermidine-condensed DNA [28].

All these electrostatic effects are also dependent on the dielectric constant of the solution. For example, condensation of DNA in salt solutions generally require the presence of ions with valence +3 or higher, but in the case of water-alcohol mixtures, condensation is observed with divalent cations as well [29]. This is due to the decrease in the dielectric constant of the solvent, which increases the force of electrostatic interactions, according to Coloumb's law [30]. The dielectric constant of the bacterial nucleoid is dependent on a lot of factors. For example, monatomic ions have been shown to decrease the dielectric constant [31][32], while zwitterionic metabolites are thought to increase it [33][34]. There is little experimental data on the dielectric constant of the bacterial cytosol, but it har been suggested to be significantly higher than that of water [35].

DNA Supercoiling

DNA supercoiling refers to the under- or overwinding of circular DNA, or stretches of DNA with contrained ends. This results in a compaction of the DNA, as the double strand will coil around itself to ease the strain of the overwinding. This is a naturally occuring strategy for DNA compaction as several enzymes have evolved for this purpose, called topoisomerases. Plasmids are circular DNA, able to acquire a variety of relaxed or supercoiled states, all of which have significantly different hydrodynamic properties [36][37]. All DNA in this work is linearized, presumably making supercoiling a negligible effect.

DNA Associated Proteins

As with the toposiomerases, other proteins have been evolved for the task of DNA compaction. In this set of experiments, the goal was investigate the activity of histone-like nucleoid structuring protein (H-NS) from *Salmonella typhimurium* in a crowded environment. It is a member of the H-NS protein family of prokaryota, which play a role in nucleoid structure and regulation of expression [38]. It generally exists as a dimer, and has the ability to self associate into higher-order oligomers [39][37]. It has a DNA-binding domain near the C-terminus, and a dimerization domain near the N-terminus [40]. It is shown to bind to the minor groove of DNA [41], preferably to adenine-thymine rich (AT-rich) regions, and structure it in two different conformations, depending on salt conditions [42]. It has been shown that in the absence of divalent ions, the protein tends to structure DNA in a rod-like manner, while in the presence of Mg^{2+}, it tends to bridge, and hence, condense DNA [26]. In this work, similar results were observed, so all experiments with H-NS included $MgCl_2$. A proposed 3D-structure of the dimer is shown in Figure 2.2 and a proposed model of the binding to DNA is shown in Figure 2.3.

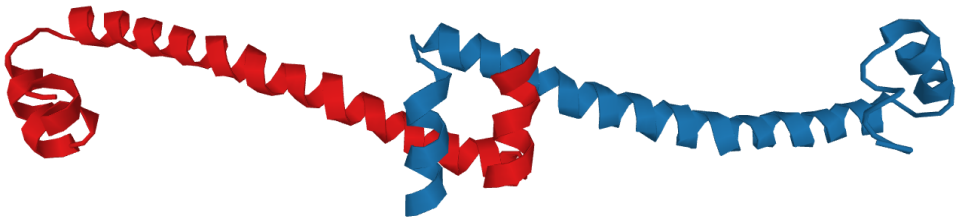

Figure 2.2: Proposed model of the dimerization N-terminal dimerization of *S. Typhimurium* H-NS protein. Amino acid residues 1-83 [43].

Crowding Effects

As shown in Figure 2.4, the bacterial interior is a quite crowded environment, both in the nucleoid and the cytoplasm in general. With a mix of molecules of different sizes occupying much of the space, the DNA is forced to compact into smaller localized regions. The cytoplasmic machinery has evolved to work in tandem with a crowded environment, which brings several significant changes. With more occupied, hence, inaccessible space, the paths for metabolites will be longer through a cell, while the path for expression mechanisms will be shorter within the localized regions of DNA. Secondly, with addition of macromolecules, the viscosity of the cytoplasm will increase significantly, compared to pure water [45]. This means that the effect of the diffusive forces will decrease, and the translational diffusion coefficient decreases according to Equation 2.1. Furthermore, a crowded environment can lead to obstructed diffusion, as with a polymer gel. If one follows the diffusion of a small solute in a gel for short time intervals, it may be similar to the diffusion through solvent, but by observing net diffusion over a longer time, it is seen that the diffusion is restrained by the presence of larger polymers. This can lead to a difference between the micro- and macroviscosity, respectively. The viscosity affects the equilibrium

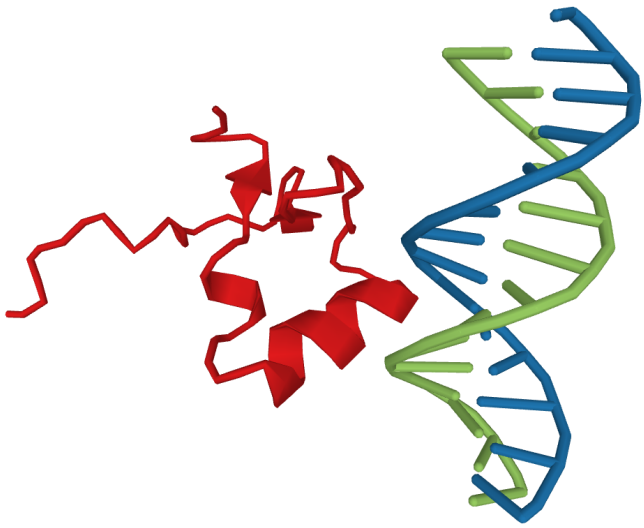

Figure 2.3: The C-terminus of Ler, a *E.Coli* H-NS protein, binding to the minor groove of DNA. Amino acid residues 56-102 [44].

of binding proteins and counter-ions; the slower diffusion will slow down the molecule movement, so they will require more time to locate and bind to the DNA complexes, but when in place, dissociation may be harder to achieve, as diffusion through the medium is more restricted. When measuring diffusion to estimate particle size, the increased viscosity has to be taken into account. The viscosity can be measured with a viscometer, or simply by measuring the diffusion of a fluorescent dye in the same crowded solution [46]. Since the dye is small enough not to undergo any significant conformational changes the crowded environment, the measured diffusion time will only depend on the viscosity of the solution.

Mass and Volume Exclusion

In bacteria, approximately 20-40% of the cytosol volume, and 40% of the cytosol mass can be attributed to biomolecules such as protein, nucleic acids, lipids, carbohydrates, all within a wide spectrum of solubilities [48]. From this arises an important consideration when mimicking a crowded environment. PEG is of relatively low specific density, with a stokes radius of 3.45 nm for 20 kDa polymers [49], while the mass of a globular protein of similar size could be three times higher [50]. From this logic it follows that 40% cellular crowding mass cannot simply be substituted by 40% polymer mass. To investigate the potential differences, two models are utilized in this laboratory investigation, one using PEG with molecular weight 3000 Da, and one using bovine serum albumin (BSA).

PEG is commonly used polymer for crowding experiments, and is provided in a whole

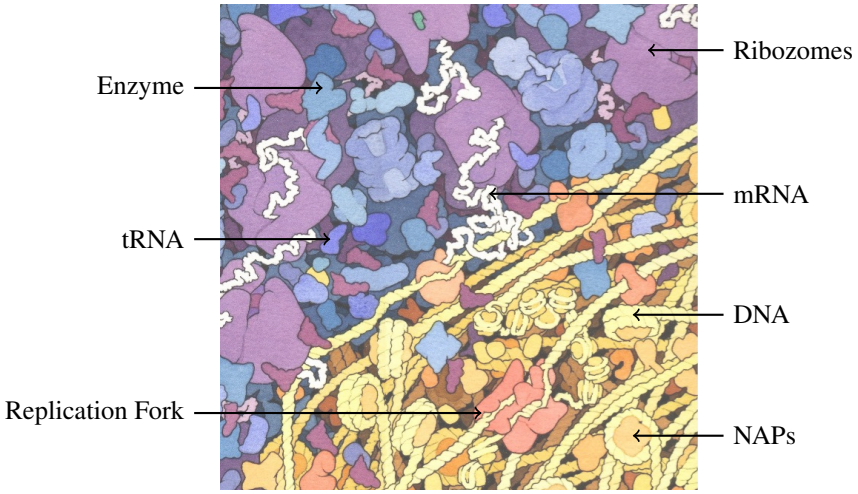

Figure 2.4: An illustration of the crowded cytoplasm of *E.coli*, showing components of the nucleoid space primarily in yellow and orange [47].

range of different molecular weights. The general formula is shown in Figure 2.5. PEG in solution will occupy space as a diffuse cloud, with a relatively low specific density.

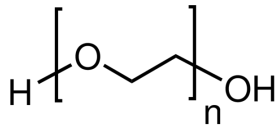

Figure 2.5: General molecular formula of PEG [51].

Bovine serum albumin, or ”Fraction V” is a globular 66.5 kDa protein isolated from cow blood. While natively responsible for exerting oncogenic pressure in blood plasma, it is often used in laboratory experiments as a protein concentration standard [80]. An illustration of the protein structure is shown in figure in Figure 2.6. It carries a net negative charge under neutral pH [52], which could lead to repulsive forces towards the negative backbone of DNA, in turn increasing the crowding effect compared to a similar, but neutral protein. It has previously been used in crowding experiments [53], has autofluorescent properties [54], and is known to aid in electrophoresis mobility shift assays (EMSAs), as it minimizes non-specific binding of protein [55][56].

Figure 2.6: Structure of BSA revealing the dense globular nature of the protein [57].

2.1.1 Diffusion and Hydrodynamic Radius

FCS measures the diffusion coefficient of a fluorescent particle. Generally, the diffusion coefficient depends on the temperature and viscosity of the sample, as well as the shape and size of the particles. They are related thorugh the Stokes-Einstein equation:

$$D_{\mathrm{T}} = \frac{k_{\mathrm{B}}T}{6\pi\eta R_{\mathrm{h}}} \tag{2.1}$$

Where D_{T} is the translational diffusion constant, k_{B} is Boltzmann's constant, T is the temperature in Kelvin, η is the dynamic viscosity, and R_{h} the radius of the particle. This holds for a spherical particle, which is assumed a satisfactory approximation for diffusing DNA in this work. The fluctuations in viscosity and radius are expected to dominate the relation, as the temperature rarely diverged more than a couple of degrees. This is a highly simplifying assumption, as solution viscosity and protein binding both are highly dependent on temperature [58][90]. Because the curve fitting from FCS acquires the translational diffusion constant D_{T}, it could be of interest to convert values into the hydrodynamic radius R_h, by reordering Equation 2.1, which gives:

$$R_{\mathrm{h}} = \frac{k_{\mathrm{B}}T}{6\pi\eta D_{\mathrm{T}}} \tag{2.2}$$

Now, as the addition of PEG and BSA will increase the viscosities of solutions significantly, this has to be taken into account, by multiplying with the relative change in viscosity. The viscosity data in this work is expressed as the ratio η/η_0 between η, the viscosity of the crowded buffer in question, and η_0, the viscosity of the solution without any crowding agents. The viscosity-adjusted diffusion constant D_v can then be expressed as:

$$D_\mathrm{v} = D_\mathrm{T}\frac{\eta}{\eta_0} \tag{2.3}$$

Now if we want to get an impression of the relative change in size, we obtain:

$$\frac{R_\mathrm{h}}{R_{\mathrm{h}_0}} = \frac{\eta_0}{\eta}\cdot\frac{D_{\mathrm{T}_0}}{D_\mathrm{T}} \tag{2.4}$$

An interesting value is the volume of the DNA, which if assumed to be spherical, could be calculated from the hydrodynamic radius, $V_\mathrm{s} = \frac{4}{3}\pi R_\mathrm{h}^3$. This can then be expressed as a relative volumetric change:

$$\frac{V_\mathrm{s}}{V_{\mathrm{s}_0}} = \left(\frac{\eta_0 D_{\mathrm{T}_0}}{\eta D_\mathrm{T}}\right)^3 \tag{2.5}$$

Error Propagation

An error estimate will be attained for both viscosity measurements and diffusion coefficients of DNA, and when it comes to multiplication and powers of measured values, the error propagation has to be taken into account. The standard errors are calculated by standard error propagation rules [59], and first the error in the viscosity estimation has to be considered, as it is dependent on the error in both η and η_0:

$$\sigma_{\eta/\eta_0} = \frac{\eta}{\eta_0}\sqrt{\left(\frac{\sigma_\eta}{\eta}\right)^2 + \left(\frac{\sigma_{\eta_0}}{\eta_0}\right)^2} \tag{2.6}$$

Some experimental values of η/η_0 is shown in Table 4.1 and 4.2. Now that values of η/η_0 with standard deviations are calculated, the error in D_v from Equation 2.3 can be attained by the same rules:

$$\sigma_{D_\mathrm{v}} = D_\mathrm{v}\sqrt{\left(\frac{\sigma_{\bar{D}_\mathrm{T}}}{\bar{D}_\mathrm{T}}\right)^2 + \left(\frac{\sigma_{\eta_0/\eta}}{\eta_0/\eta}\right)^2} \tag{2.7}$$

Where σ_{D_v} is the standard deviation in D_v, $\sigma_{\bar{D}_\mathrm{T}}$ is the standard deviation in the measurement average $\bar{D}_\mathrm{T}$, and $\sigma_{\eta_0/\eta}$ is the standard deviation in η_0/η. Furthermore, when calculating the volumetric change $V_\mathrm{s}/V_{\mathrm{s}_0}$ according to Equation 2.5, the power has to be taken into account by the same rules, which generally state for $a = b^n$:

$$\frac{\sigma_a}{|a|} = |n|\frac{\sigma_b}{|b|} \tag{2.8}$$

Which for the power of three in this case gives:

$$\sigma_{V_s/V_{s_0}} = 3\cdot\frac{V_s}{V_{s_0}}\cdot\frac{\sigma_{D_\mathrm{v}}}{D_\mathrm{v}} \tag{2.9}$$

Mass Dependence

Mass dependence has to be considered, being that the binding of protein presumably increases the mass of the DNA complex significantly. Free DNA, and DNA-H-NS complexes, will differ significantly in weight. Assuming the mass contribution of the DNA dye to be negligible, this ratio is:

$$\frac{m_1}{m_0} = \frac{\langle m_{\mathrm{DNA}} \rangle + \frac{m_{\mathrm{H-NS}}}{N_{\mathrm{H-NS}}}}{\langle m_{\mathrm{DNA}} \rangle} \tag{2.10}$$

Where m_0 and m_1 is the weight of the DNA complex before and after binding of the protein, respectively. $\langle m_{\mathrm{DNA}} \rangle$ is the average mass of a DNA basepair, $m_{\mathrm{H-NS}}$ is the molecular mass of H-NS protein and $N_{\mathrm{H-NS}}$ is the number of pase pairs per H-NS molecule under saturation. With $m_{\mathrm{H-NS}} = 15,540$ Da, $\langle m_{\mathrm{DNA}} \rangle = 607.4$ Da [60], and protein saturation at one H-NS per 12 bp [61]. This yields:

$$\frac{m_1}{m_0} = \frac{607.4 + \frac{15{,}540}{12}\mathrm{Da}}{607.4\mathrm{Da}} = 3.132 \tag{2.11}$$

It would be fair to suspect that a three-fold increase in the weight would affect the diffusion time. The Stokes-Einstein relation however, clearly does not depend on mass, as this equation concerns particles of sufficiently higher density than the surrounding fluid [62]. Because the appproximate density of protein and DNA is close to that of water, at approximately 1.3-1.7 g/cm^3 [63][64], the effects of density should be taken into account. The Stokes-Einstein relation can be modified through the Basset-Boussinesq equation [65]. The mass-adjusted diffusion constant can then be expressed as:

$$D = D_{\mathrm{E}} \left(1 + 2\frac{m_{\mathrm{f}}}{m}\right) \tag{2.12}$$

Where D_{E} is the mass-independent Stokes-Einstein diffusion constant, while m and m_{f} is the mass of the protein-DNA complex, and the mass of the fluid it displaces, respectively. We can see that if the diffusing particle is of the same density as water, this yields a three-fold increase in the diffusion constant, while for a very dense particle, $m \gg m_{\mathrm{f}}$, $D \simeq D_{\mathrm{E}}$. A low density particle $m \ll m_{\mathrm{f}}$ diffuses rapidly, as one would suspect. Protein and DNA is denser than water, but the hydration of the molecules leads to a decrease in density, approaching the limit of $D \simeq 3D_{\mathrm{E}}$. The density of protein is generally lower than DNA, which would make the DNA-H-NS complex of higher mass, but lower density. However, free DNA will expectedly adsorb more solvent than the protein-rich condensed DNA coil, an effect which will compete with the lower density of the protein. In conclusion, this effect will likely be negligible, and as relative results are mostly considered, the density correction is largely unimportant.

2.2 Fluorescence

In short, fluorescence is the ability of a material to be excited by light of one wavelength, and emit light of another wavelength during de-excitation. This enables for many creative techniques in biophysical investigation, and in this work, most measurement procedures,

including FS, FCS, expression assays, and all gel electrophoresis imaging rely on fluorescence. The possibility of illuminating with one wavelength and measuring emission of another is of great importance, as it allows for fluorescent dyes to be located specifically. Because these dyes have higher or lower affinities for different biological molecules, this enables location and imaging of specific intracellular targets. There are also naturally occurring fluorescent proteins, such as green fluorescent protein (GFP), which enables relatively easy confirmation of transformation through fluorescence spectroscopy.

2.3 Fluorescence Spectroscopy

FS investigates the fluorescent emission and absorbance of a sample. The main components are a laser and a detector, both working over a span of wavelengths. This way, emission spectra can be obtained for a given excitation wavelength, or excitation spectra for a given emission wavelength. The most common setup in biophysics is a multi-well plate reader, which excites the samples in each well, and records the emitted fluorescence.

2.3.1 Dye Exclusion

Many of the dyes used in DNA investigation yield a more intense emission upon binding to DNA, and this is also the case with GelStar, the dye used in this FS work. An example of the emission spectra of free and bound GelStar is shown in Figure 3.4, where this difference is apparent, not only in intensity, but also in the shape of the curve. Dye exclusion utilizes this difference, as the intensity from a sample is now a measure of how much bound dye there is, and hence, of how much free DNA there is in the solution for the dye to bind to. Condensed DNA will be less accessible to the dye, so the emission will be lower in the samples where condensation occurs.

2.3.2 Expression Assays

In order to quantify the biological effect of protein and crowding on DNA, cell-free protein synthesis is a useful tool. By using a model cytoplasm instead of living expression vectors, a consistent yield can be attained, and expression under different conditions can effectively be compared. To ease detection of expressed protein, the gene used in this work translates to a GFP, which is readily detected by fluorescence spectroscopy. This makes for a relatively accurate dye-free measurement of net expression, as there is no rogue dye that can bind to other factors and lead to confusing changes in emission. Expression requires numerous factors, including ribonucleotides and RNA polymerase for transcription, and ribozomes and amino acids for translation. These reagents are to be added in suiting ratios and concentrations, along with the right buffer conditions, energy substrates and cofactors. This process is tedious and expensive to do, so ready-made kits containing all these ingredients are commercially available.

There are many important considerations when using cell free protein synthesis to investigate DNA-protein-crowding interaction. Firstly, commercial expression kits are already crowded by the expression machinery, and could contain condensing agents [66]. So in

this way, any additional ingredients will be added on top of an already crowded and somewhat condensed state of DNA. Therefore, these assays will not lead to very general results, but can be assessed as additional evidence. Secondly, if an agent is found to reduce expression, this could be due to interaction with the RNA transcript, proteins or other factors in the mixture, and not necessarily interaction with the DNA. One way to investigate inhibition of transcription, RNA can be quantified and compared to the protein production. To quantify RNA production, a dye with high affinity to RNA can be added after measuring GFP activity. A new emission measurement will reveal information about the RNA production in the sample. Other methods like RNA gel electrophoresis or real-time PCR could also reveal information about mRNA production [67].

2.4 Fluorescence Correlation Spectroscopy

FCS is one of the many applications of the confocal laser scanning microscope (CLSM), which is reviewed briefly in Section 2.4.1.

2.4.1 Confocal Laser Scanning Microscope

CLSM is an optical microscope that can use fluorescence and phosphorescence, in addition to absorption and reflection, to investigate matter. It manipulates a laser beam to illuminate a focal volume in a sample and utilizes an aperture confocal to the light source aperture in order to eliminate emission from focal planes in the sample, as shown in Figure 2.7. Samples can be subjected to dyes with differing optical properties and binding specificities, so that specific biological components can be recorded separately in the same sample. Using this procedure, emission from protein, membrane, nucleotides, or any other specific target for a dye can be recorded in turn to create a composite image. Because of the spatially limited focal volume, it can also be used to create a stack of images from a range of focal depths in the sample, revealing three-dimensional structure.

2.4.2 Correlation Spectroscopy

FCS is based on a time-resolved recording of the emission from the focal volume at constant illumination. As fluorophores enter and exit the volume, the light intensity will fluctuate accordingly, and reveal dynamic properties of the dye-molecule complexes. An illustration of a fluorophore diffusing through the focal volume is shown in Figure 2.8.

In theory, a statistical distribution of the time required for particles to traverse the volume could yield an average diffusion time, reflecting the real diffusion time of the particle. There are numerous factors to be considered in this model; The shape and size of the focal volume has several effects on the correlation. It will take longer for a particle to diffuse through a larger volume, and even longer if it diffuses along a larger cross section of the presumably ellipsoid focal volume [68]. The ellipsoid radii, z_0 and w_0, shown in Figure 2.8 are therefore necessary to obtain, if absolute diffusion coefficients are of interest. The values are attainable by calibration with a concentration series of a fluorophore of known diffusion constant, but this is a relatively tedious procedure, and since measuring

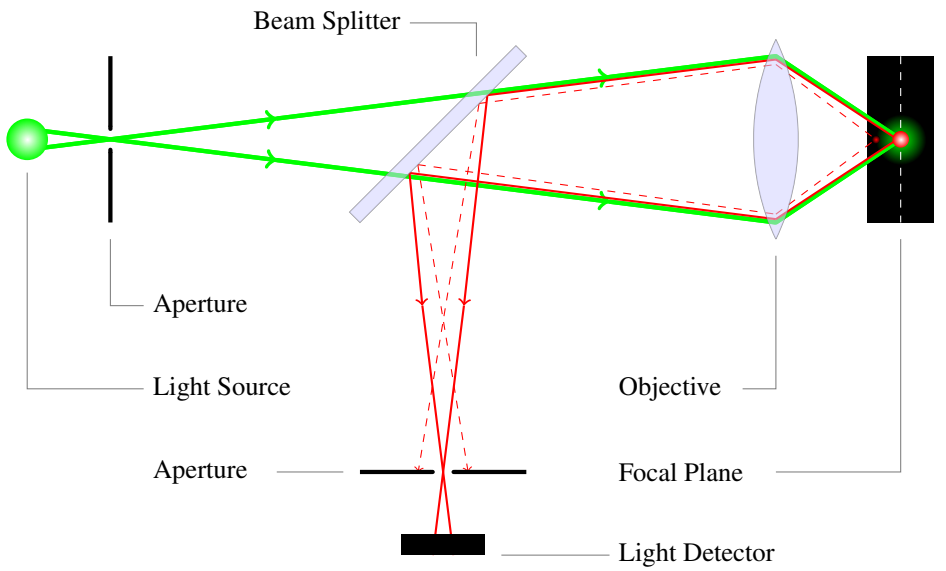

Figure 2.7: The theoretical setup behind the confocal microscope. As shown, emission from other depths than the focal plane will be eliminated by the secondary aperture. Illustration drawn with TikZ.

relative compaction of DNA is the scope of this laboratory work, normalized data will suffice. In this case, some values can normally be set as constant, with a ratio $\kappa = z_0/w_0$ set between 5-10. But because the DNA complexes are large, $R_{\mathrm{G}} \simeq 213$ nm for 5.9 kbp [69], compared to the focal volume $V \simeq 1\mu\mathrm{m}^3$, the software will recognize the κ to be closer to one. This is because the relative difference in diffusion time between complexes that traverse shorter or longer paths through the effective volume will be smaller. Another important consideration when it comes to large particle size, is that the average number of diffusing complexes can be lower. The correlation software designers have stated that the ideal concentrations for FCS is 1-20 nM [70], an average of 0.6-12 particles in a 1 fl focal volume. In the case of lower averages than this, it is necessary to increase the measurement duration to obtain adequate statistics for analysis.

Another significant factor is the fraction of dye that shortly after entering the focal volume wind up in dark states. The main dark states are photobleaching and triplet excited states, the latter which is due to an electron inverting its spin as it excites, preventing it from de-exciting to its original orbital where there already is an electron of its spin, according to the Pauli exclusion principle [71]. This will give rise to an additional, seemingly shorter diffusion time, as the duration of the emission ends before the particle actually exits the volume. The dyes used in these FCS-measurements, YOYO-1 and Alexa 488, are highly photostable, which means photobleaching can largely be diminished by correctly adjusting the laser intensity.

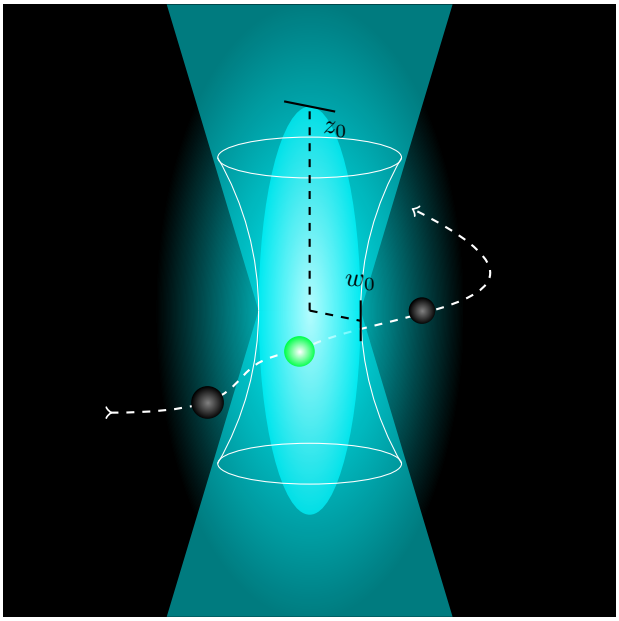

Figure 2.8: Focal volume V_{Eff} of the fluorescence microscope. The radii z_0 and w_0 are of importance when analysing the correlation of the fluorescence fluctuation. Approximate colors of 488 nm Argon excitation light and 525 nm excitiation maxima of Alexa-488. Illustration drawn with TikZ.

2.4.3 Autocorrelation Function

Fluctuation in the emission intensity from the focal volume corresponds to the movement of fluorophore through it. This data can be interpreted by using the autocorrelation function (ACF):

$$G(\tau) = \frac{\langle \delta I(t) \delta I(t+\tau) \rangle}{\langle I(t) \rangle^2} = \frac{\langle I(t) I(t+\tau) \rangle}{\langle I(t) \rangle^2} - 1 \tag{2.13}$$

Where $I(t)$ is the intensity at time t, τ is the lag-time, $\delta I(t) = I(t) - \langle I(t) \rangle$ is the deviation from the mean intensity at time t, and $\delta I(t+\tau) = I(t+\tau) - \langle I(t+\tau) \rangle$ is the deviation from the mean intensity at time $t + \tau$. Naturally, correlation functions are calculated on a computer, using either customized scripts, or a commercially available interface such as SymphoTime, used in this work. An example ACF is shown in Figure 2.10.

Curve-Fitting and Triplet State Correction

The ACF can reveal several properties of the system. The procedure is to fit a theoretical function to the measured ACF, which is dependent on several factors, such as the focal volume and average diffusion times. This is also done using signal analysis software, and several curve fit models are available, depending on the complexity of the system. As mentioned, triplet states can be a nuisance in FCS, but there are scripts available that include triplet state corrections. The corrected expression used for this analysis states:

$$G(\tau) = \left[1 - T + Te^{-\frac{\tau}{\tau_{\mathrm{T}}}}\right] \sum_{i=1}^{n} \rho_i \left(1 + \frac{\tau}{\tau_i}\right)^{-1} \left(1 + \frac{\tau}{\tau_i \kappa^2}\right)^{-\frac{1}{2}} \tag{2.14}$$

$G(\tau)$ is a theoretical continuous distribution of particles for the variable lag time τ (ms), for a sample of n different species. Several factors are obtained by the curve fit; T is the fraction of molecules in dark states, τ_{T} (ms) is the average time a molecule spends in dark states, or the triplet state relaxation time. Theoretically, this number should be less than 10 ns, but can in extreme cases be increased slightly if the curve fit requires it. $\kappa = \frac{z_0}{w_0}$ is the ratio between the height and width of the focal volume. ρ_i and τ_i is the amplitude contribution and average diffusion time of the i^{th} diffusing species, intuition states that these are related to the height of $G(\tau)$ and the horizontal position of the descending slope, respectively. From these parameters, key values can be calculated, like the focal volume $V_{\mathrm{Eff}} = \pi^{\frac{3}{2}} w_0^2 z_0$ (fl), mean molar concentration $\langle C \rangle = \frac{\langle N \rangle}{V_{\mathrm{Eff}} N_{\mathrm{A}}}$ (nM), and the diffusion coefficient $D_i = \frac{w_0^2}{4\tau_i}$ ($\mu\mathrm{m}^2/\mathrm{s}$). Equation 2.14 is valid for multiple diffusing species, and curve fitting was in this case satisfactory by assuming one or two species. The additional species is needed due to the significant contribution of smaller DNA-fragments and free dye in the sample.

2.4.4 Detector Afterpulsing

The first challenge in the search for a FCS measurement protocol with consistent results, was the detector afterpulsing. As an avalanche photo diode (APD) detects a photon, it

generates afterpulses, which are highly correlated to the original detection. This gives rise to a peak in the lower time-scales of the ACF, as shown in the measurement of rhodamine 6G (R6G) in Figure 2.9.

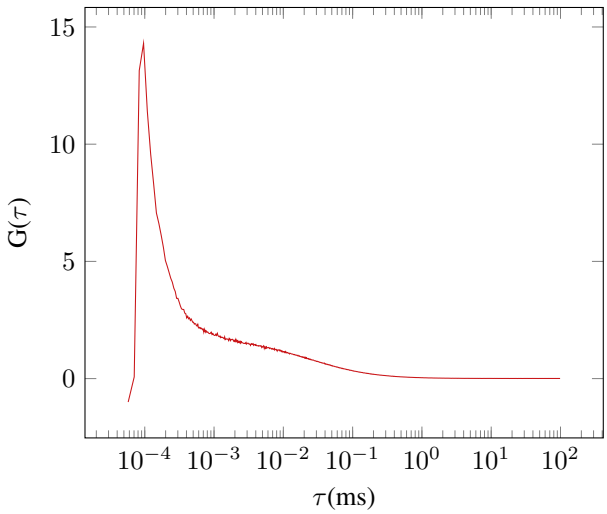

Figure 2.9: Unaltered ACF of 8 nM R6G. The peak arises due to the significant afterpulse of the instrument.

There are several ways to account for this erroneous peak, including fluorescence lifetime filtering [72], two-channel cross-correlation [73], or simply increasing the minimum lag-time, as afterpulses generally are faster than the fluctuations due to diffusion of matter. The results in this report were subject to the latter procedure, and the truncation of the curve in Figure 2.9 is shown in Figure 2.10. The minimal lag time was set to 0.003 ms, approximately the time when the sharp peak in Figure 2.9 ends.

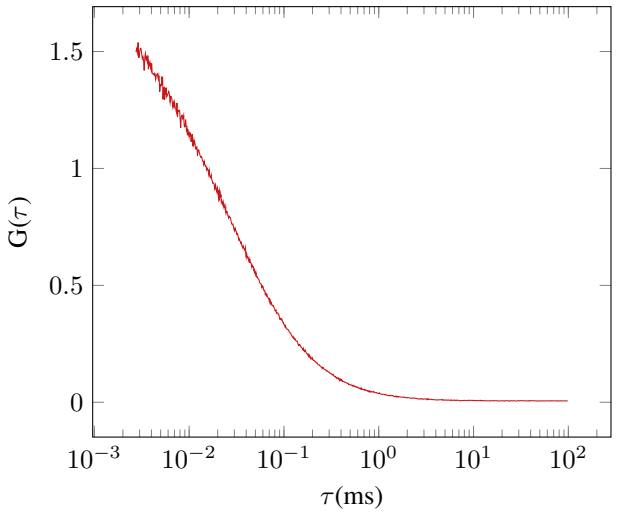

Figure 2.10: Truncation of the ACF of 8 nM R6G.

2.4.5 Bootstrapping and Weighted Arithmetic Mean

Impurities, dust and aggregates of fluorescent particles can be a major problem in FCS. The passing of only one sizable aggregate through the focal volume can deteriorate the quality of a measurement of several minutes. When an average and error estimate is calculated, this will yield poor accuracy and high standard deviations. Hopefully, there are options to minimize this interference. One way is to monitor the auto-correlation curve carefully during measurement and noting the time points where big deviations occur and cut them from the time trace before curve-fitting. Similarly, one could do shorter measurements and delete the curves where deviations were present. A less subjective method, and the method used in this research, is to utilize error estimates from the curve fits to calculate a weighted arithmetic mean of the measurements, so that "bad" curve fits do not influence the mean as much as the "good" ones. For this, a statistical re-sampling tool called bootstrapping can be used [74]. In short, after a curve-fit is obtained, the auto-correlation function is re-sampled with replacement, and the theoretical curve is compared to the new data set [75]. A good match to these re-sampled curves indicate a "good", unambiguous curve-fit. A 68% confidence interval can then be obtained, reflecting the standard deviation of the fit. This whole ordeal is done by the curve-fitting software, and the exact algorithm is beyond the scope of this thesis. It is worth noting that this error estimate is not an error estimate for the measurement, but for the theoretical curve fit upon the measurement, so to obtain a standard deviation for the sample measurement, several recordings are still needed. The bootstrap error estimate σ_{D_i} for each measured diffusion constant D_i is used in a weighting factor $w_i = 1/\sigma_{D_i}$ to calculate the weighted arithmetic mean $\bar{D}_{\mathrm{T}}$ of the measurements. For instance, the second curve fit in Figure 4.10 has an error estimate of ± 0.293, which means it will not affect the mean as much as the first curve fit, with its error of ± 0.177. With an n number of curve fits, the weighted arithmetic mean of the measured

values is given by:

$$\bar{D}_{\mathrm{T}} = \frac{\sum_{i=1}^{n} w_i x_i}{\sum_{i=1}^{n} w_i} = \frac{\sum_{i=1}^{n} \frac{1}{\sigma_{D_i}} D_i}{\sum_{i=1}^{n} \frac{1}{\sigma_{D_i}}} \tag{2.15}$$

The same is done to acquire the weighted standard deviation, where results with poor theoretical curve fits influence the standard deviation less than better curve-fits. This way, the standard deviation will more closely reflect the real deviations in the sample:

$$\sigma^2_{\bar{D}_{\mathrm{T}}} = \frac{\sum_{i=1}^{n} w_i (D_i - \bar{D}_{\mathrm{T}})^2}{\sum_{i=1}^{n} w_i} = \frac{\sum_{i=1}^{n} \frac{1}{\sigma_{D_i}} (D_i - \bar{D}_{\mathrm{T}})^2}{\sum_{i=1}^{n} \frac{1}{\sigma_{D_i}}} \tag{2.16}$$

2.5 Atomic Force Microscopy

Atomic force microscopy (AFM) is an advanced technique that can achieve resolutions in the order of 1 nm. The instrument would require a lengthy section on its own to do it justice. Nevertheless, in this work it was used only in its most basic setup with dry samples and tapping mode, and it was featured mostly for confirmation that the purified H-NS protein was active. Thus, a thorough theoretical introduction is beyond the scope of this thesis.

2.6 Electrophoresis Mobility Shift Assays

An EMSA is a common electrophoresis technique used to study protein-DNA and protein-RNA interactions. It utilizes the difference in the mobility of a DNA or RNA fragment upon binding to protein, which decreases the migration of the polynucleotide through a gel. In order to maintain binding, recommended running voltages are generally lower than with regular DNA gel electrophoresis, and care has to be taken to inhibit denaturation of the protein, such as buffer and stain optimization, SDS (sodium dodecyl sulfate)-free loading dyes, as well as pre-running or refrigeration to maintain temperature control [76].

Chapter 3

Materials and Methods

3.1 Cell Culture and Plasmid Purification

The objective for the plasmid purification seemed trivial: to standardize a protocol for acquiring pure, linear dsDNA with 4-7 kbp length, preferably translating to a easily quantifiable protein. This turned out to be a more time consuming task than expected.

3.1.1 Plasmid for Initial Experiments

For use in initial tests and standardization of measurement procedure, plasmid pTA16-PT7-gfpmut3 (6288 bp) was chosen because it includes a gene for green fluorescent protein (GFP), which is easily quantifiable by fluorescence spectroscopy. The plasmid was expressed in bulk amounts and purified from DHα5 *E.Coli*. The already-transformed bacteria were generously provided by Simone Balzer Le at the Department of Biotechnology and Nanomedicine at Sintef. A map of the plasmid is shown in Figure 3.1, which includes a T7 promoter encoding for a Green Fluorescent Protein (GFP) variant, genes for kanamycin resistance, a single restriction site for NdeI, and it yields a copy number of about 20-30. Mother cultures were incubated overnight on kanamycin plates, colonies were selected and incubated in liquid medium. All incubation was performed at 37 °C, for approximately 16 hours. All extraction of plasmid DNA was done with Promega Wizard® Plus SV Minipreps DNA Purification System according to producer protocol [77], followed by gel electrophoresis inspection and measurement of DNA concentration on NanoDrop, described further in Section 3.4.1. The plasmid was subsequently linearized by digestion with the restriction enzyme NdeI and CutSmart™ buffer, for 3 hours at 37 °C, and was again investigated by gel electrophoresis. The digestions were selected and purified by phenol/chloroform extraction [78] followed by ethanol precipitation. This plasmid was used in the initial FS measurements, to map interesting concentration ranges for PEG and spermine. Several issues were encountered with this protocol; firstly, the yield was too low for the amount of DNA needed for the FS and FCS investigation, due to the low copy-number of the plasmid. Secondly, the phenol/chloroform protocol resulted in high

contamination and low DNA concentration, again to such an extent that the samples were sub-optimal for the desired measurements. This plasmid was not included in any results in this report, but was important to learn a great deal in the purification and manipulation of plasmid DNA.

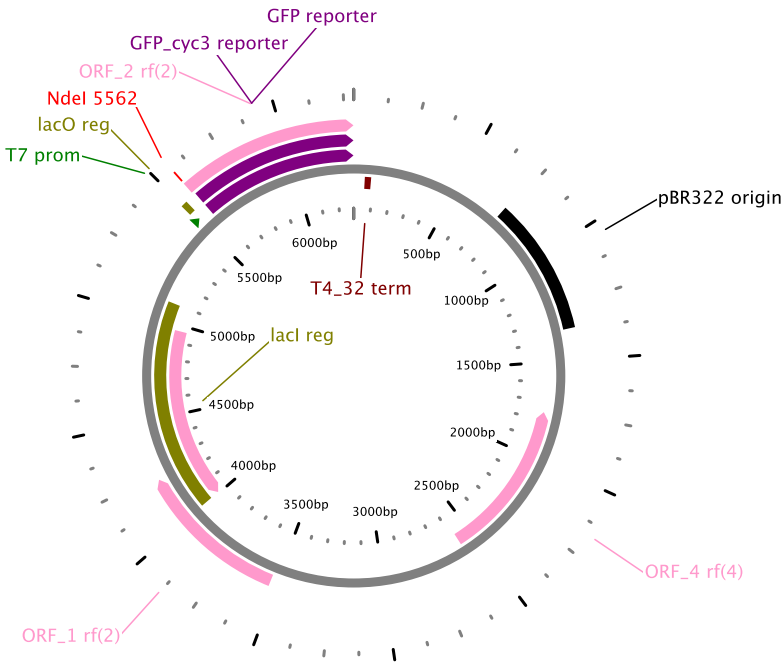

Figure 3.1: Map of plasmid pTA16-PT7-gfpmut3.

3.1.2 High Copy-Number Plasmids

To fix the problem of low yield, two other GFP plasmids of higher copy-number were investigated, pSB-M2g-1-17 (6010 bp) and pSB-M1g-cop271 (7828 bp), plasmid maps shown in Figure 3.2. These were also harvested from DHα5 *E.Coli* cells, and included genes for kanamycin resistance. A liquid medium culture was inoculated at 37 °C for 16 hours, and the plasmids were extracted. The DNA concentrations from both strains were high, the highest being the pSB-M2g-1-17, making it the preferred source of DNA. To linearize the plasmid, digestion was tested with both NdeI and BamHI-HF, both giving single fragments. NdeI and CutSmart™ was chosen for bulk inoculation, as it was available in reasonable quantities. After digestion, the plasmid was again purified with phenol/chloroform extraction, but due to the unreliable results obtained with this process, the Promega Miniprep [77] was used for the final DNA stock. The result was a working stock of relatively pure 17 ng/µl pSB-M2g-1-17. This DNA was used in all FS, and on the combined effects of PEG and spermine in FCS.

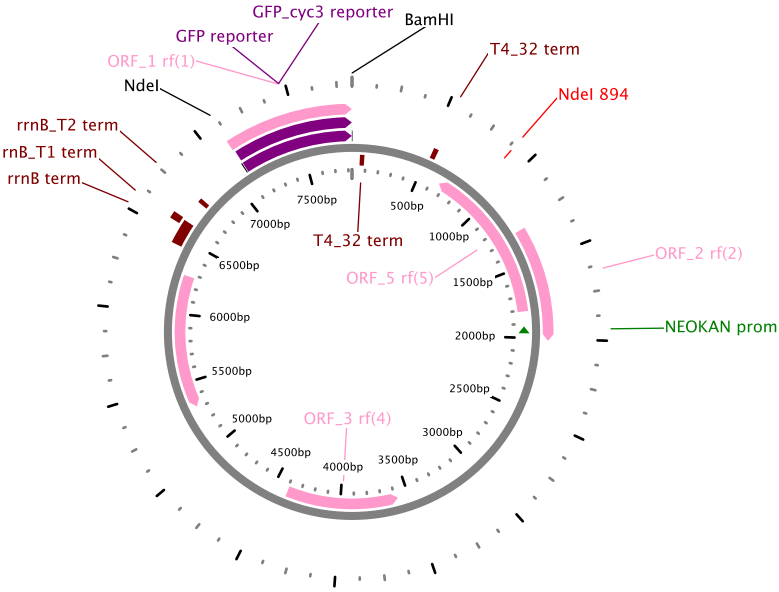

(a) pSB-M1g-cop271

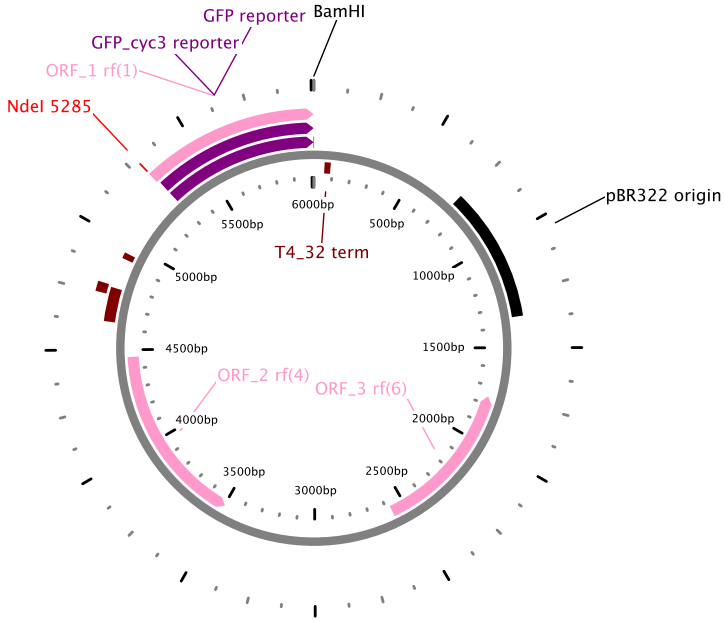

(b) pSB-M2g-1-17

Figure 3.2: Maps of high copy number plasmids.

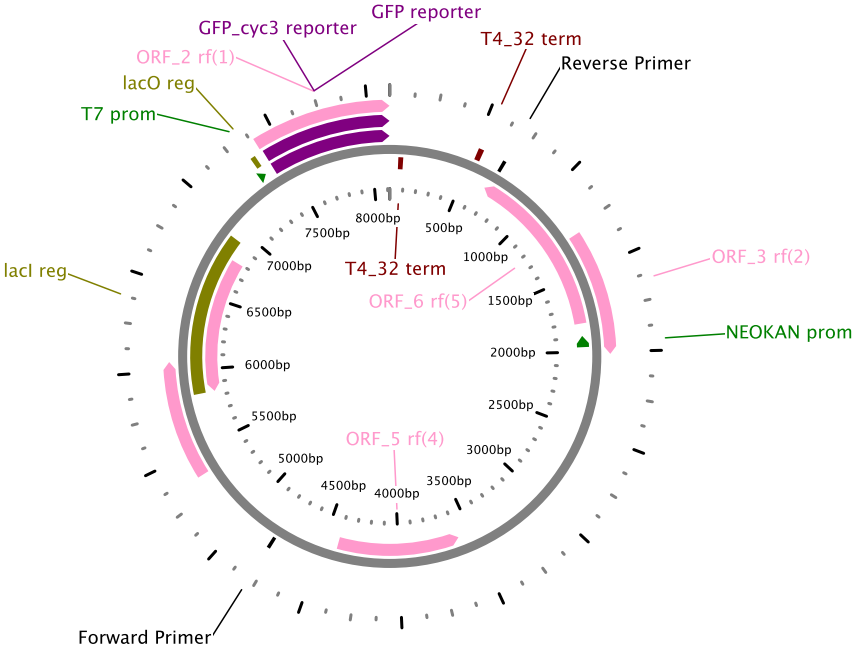

Figure 3.3: Map of plasmid pSB-E1g, showing GFP gene and primer positions.

3.1.3 PCR Product

The process of purifying plasmid DNA from culture is a relatively tedious endeavor, and called for the design of a PCR protocol. At the same time, a PCR product could be made to include the GFP gene and the promoter sequence needed. Plasmid pSB-E1g (8117 bp) was chosen as a template, and like the other plasmids, it included the quite common bacterial T7 promoter and a gene for GFP. Sequence and specifics of the primer pair is shown in Table3.1, and their positions are indicated on the plasmid map in Figure 3.3, spanning an amplicon length of 4017 bp. Phusion® polymerase was chosen for the task, for speed and high fidelity, and the protocol is shown in Subsection 3.1.4, which yielded 30 µl of 100-400 $\mathrm{ng}/\mu\mathrm{l}$ pure DNA, per 50 µl PCR reaction. This DNA was used in cell-free expression assays and EMSAs.

Table 3.1: Specifics of the primer pair used in PCR protocol.

Primer	Sequence	Position	Annealing Temp.
Forward	5' GCTGGCCGATAAGCTCTAAG 3'	4779	55 °C
Reverse	5' GGTGCATTGCAAACGCTAGG 3'	679	55 °C

Fluorescent Nucleotides

Some problems arose when the effects of H-NS was investigated using DNA-binding dyes. At μM concentrations of H-NS, both the GelStar and the YOYO-1 interacted significantly with the protein, which resulted in fluorescently labeled oligomers of H-NS and as well as DNA, making FCS measurements very ambiguous, and dependable results impossible. A solution was to do PCR with fluorescent nucleotides, yielding a covalently stained DNA stock. ChomaTide® dUTPs with covalently bound Alexa 488 dye was chosen on the basis of high photo-stability and practical excitation wavelength for the argon laser used in FCS. Incorporation of dUTPs requires a DNA polymerase without proof-reading abilites, so a PCR protocol for *Taq* DNA polymerase was designed, shown in Subsection 3.1.4. This PCR product was used in all FCS measurements with H-NS.

3.1.4 PCR Protocols

All thermocycling was executed with an Eppendorf Mastercycler Gradient (Eppendorf No. 950000015).

Phusion PCR Components

1. 33 µl Nuclease-free water
2. 10 µl 5×GC Phusion buffer
3. 1 µl dNTP mix 10 mM
4. 2.5 µl Forward Primer 0.5 μM
5. 2.5 µl Reverse Primer 0.5 μM
6. 1 µl Template DNA 100 $ng/\mu l$
7. 0.5 µl Phusion® DNA Polymerase

***Taq* PCR Components**

1. 32.05 µl Nuclease-free water
2. 5 µl 10× *Tac* Buffer
3. 1 µl dATP 10 mM
4. 1 µl dCTP 10 mM
5. 1 µl dGTP 10 mM
6. 3.75 µl dTTP 2 mM
7. 2.50 µl ChromaTide dUTP 1 mM
8. 2.50 µl Forward Primer 0.5 μM
9. 2.50 µl Reverse Primer 0.5 μM
10. 1.2 µl Template DNA 100 $ng/\mu l$
11. 0.5 µl *Taq* DNA Polymerase

Phusion PCR Thermocycling

1. Initial denaturation at 98 °C for 30 s
2. Cycle denaturation at 98°C for 10 s
3. Annealing at 60 °C for 20 s
4. Elongation at 72 °C for 2:00 min
5. Repeat step 2→4 for 35 cycles
6. Final extension at 72 °C for 8:00 min
7. Hold at 4 °C

***Taq* PCR Thermocycling**

1. Initial denaturation at 95 °C for 30 s
2. Cycle denaturation at 95 °C for 25 s
3. Annealing at 60 °C for 20 s
4. Elongation at 68 °C for 4:00 min
5. Repeat step 2→4 for 25 cycles
6. Final extension at 72 °C for 5:00 min
7. Hold at 4 °C

3.1.5 Closing Remarks on DNA Stock

All the procedures and different plasmids were important in the learning process, but after mentioning 4 plasmids and two PCR protocols, some things should be emphasized for clarity. Ultimately, only two different DNA strands were used in this report. Firstly, the linearized 6010 bp psbM2g-1-17 plasmid was only used for FS, and all FCS measurements

that include spermine. Results from these investigations are referred to as *previous data*, featured in Section 4.1. The DNA used for everything else was the 4017 bp PCR product from plasmid pSB-E1g, but the covalently stained version was used in FCS measurements. These investigations are referred to as *new results*, featured in section 4.2.

3.2 Solvents, Enzymes, Crowding, and Nucleoid-Associated Protein

All water used was of the ultrapure Milli-Q (MQ) standard, defined by its resistivity of 18.2 $M\Omega \cdot \mathrm{cm}$ at 25 °C. The only exception was when using MiniPrep kits [77], where nuclease-free water provided with the kit was used instead.

Buffer Solutions

A main buffer mixture of 200 mM Tris and 3 M KCl was prepared. As mentioned in Section 2.1, DNA condensation was not observed in the absence of divalent ions, so for experiments with H-NS, another stock was made with the same concentrations, but it also included 100 mM $MgCl_2$. All buffers were prepared with MQ water and filtered with a 0.22 μm Millipore® Stericup™ Express PLUS.

Restriction Enzymes

All restriction enzymes were from New England Biolabs. BamHI-HF® (cat.# R3136S) and NdeI (cat.# R0111S) were used successfully with CutSmart™ buffer (cat.# B7204S).

Polyethylene Glycol

BioUltra poly(ethylene glycol) of approximate molecular weight 3,000 Da was purchased from Sigma-Aldrich, (cat.# 81227-250G) and prepared to a main stock of concentration 400 mg/ml, kept at -4 °C.

Bovine Serum Albumin

$\geq$98% BSA was acquired from Sigma-Aldrich (Cat.#A7906-100g), and prepared to a main stock of 270 mg/ml, kept at -20 °C.

Spermine

$\geq$99% Spermine was purchased from Sigma-Aldrich (cat.# 85590-5G), and diluted to 1 mM main stock, kept at -20 °C.

H-NS Protein

Plasmid PSSA2 encoding for *Salmonella typhimurium* H-NS, including a 6× histidine tag at the C-terminal was provided by William Wiley Navarre of The Department of Molecular Genetics at the University of Toronto. The plasmid was used to transform *E.coli* which

was grown at 37 °C overnight, until an approximate optical density of 0.6 at 600 nm was achieved. Over-expression of H-NS was induced by adding a final concentration of 0.1 mM Isopropyl β-D-1-thiogalactopyranosid (IPTG) and incubating at 18 °C overnight. The cells were harvested by centrifugation, and the protein was purified using Qiagen Ni-NTA fast start kit [79]. The buffer for the final protein was exchanged to 20 mM Tris pH 7.2, 300 mM KCl and 10% glycerol, and the stock was parted into aliquots and stored at -20 °C. The protein was investigated by SDS polyacrylamide gel electrophoresis (SDS-PAGE) and excised bands were delivered to Davi de Miranda Fonseca at the Department of Cancer Research and Molecular Medicine at NTNU for protein mass spectrometry. This investigation identified *S.typhi* H-NS with high confidence as the major protein. The concentration was estimated to be around 1.5 $\mu g/\mu l$, or 95μM by Bradford protein assay [80].

Fluorescent Dyes

For FS dye exclusion assays, GelStar™ Nucleic Acid Gel Stain 10,000$\times$ solution in dimethyl sulfoxide (DMSO) was purchased from Lonza Rockland, Inc. (cat.# 50535). It was then diluted in MQ water to 100$\times$ working stock. GelStar™ was chosen beacuse of its relatively lower binding affinity to DNA, enabling its release when protein and other agents bind to DNA. The excitation and emission maxima of the dye is 493 nm and 527 nm when bound to DNA, respectively, and there is a significant increase in intensity, compared to that of the free dye.

For standardization of FCS protocol, rhodamine 6G $\sim$ 95% from Sigma-Aldrich (cat.# R4127) was used. It was diluted to 8 nM in MQ-water. The dye has an experimental excitation and emission peak at 530 nm and 566 nm, respectively. The R6G stock and prepared samples were mixed vigorously, as the dye tends to form dimers or higher-order aggregates in aqueous solutions [81].

For FCS in previous data, YOYO-1, 1 mM in DMSO was purchased from Life Technologies (cat.# Y3601), and diluted to 1 µM working stock. This intercalating dye was selected because of high binding affinity and photostability, as well as a 3,200 fold increase in fluorescence intensity upon binding to dsDNA [82], which should yield a low signal-to-noise ratio, even with a moderate amount of free dye in the solution. The dye has absorption and emission maxima at 491 nm and 509 nm when bound to DNA, respectively.

ChromaTide® Alexa 488-stained dUTP for incorporation by PCR was bought from Life Technologies (cat.# C-11397).

Expression Assay Kit

TnT® Quick Coupled Transcription/Translation System (cat.# L1170) was purchased from promega. This kit provides 40 reactions of 50 µl, but allows for reduced sample size. The main component in the kit is the T7 Quick Master Mix, which includes everything necessary for expression; ribonucleotides, enzymes and amino acids, but no methionine. The

methionine is included separately in the kit, in order to control expression. The original idea was to add an RNA-specific dye after GFP measurement to quantify mRNA production as well, but this dye suffered from exclusion upon addition of crowding and condensing agents.

3.3 Sample Preparation

3.3.1 Fluorescence Spectroscopy

For FS, a minimum sample size of 50 µl was found to be required for sufficient emission intensity and minimization of error. The final concentration of the samples were 2 ng/µl linear psbM2g-1-17 DNA, 10× GelStar™, 300 mM KCl and 20 mM Tris. The DNA and dye were incubated alone for 1 hour in darkness, before being added to the sample. Consecutively, spermine and PEG were added, and set to incubate in the dark for 1 more hour.

PEG concentrations varied from 0-200 mg/ml, and a control with 200 mg/ml PEG with no DNA was examined to detect any interaction between PEG and GelStar.

Spermine concentrations varied from 0-150 mM, and controls with 150 mM spermine and no DNA were examined to detect any interaction between the spermine and GelStar.

The samples were loaded in Nunc-Immuno™ MicroWell™ 96 well polystyrene plates from Sigma-Aldrich (cat.# P8616). Three samples were prepared for each concentration.

3.3.2 Fluorescence Correlation Spectroscopy

To reduce sample sizes, silicone isolators from Grace Bio-Labs were used (cat.# GBL666108), allowing for 5 µl samples and minimizing the effects of evaporation. The final concentration of DNA was 2.25 $\mathrm{ng}/\mu\mathrm{l}$. When using covalently stained DNA, no incubation of dye was necessary. Incubation with YOYO-1 was done at room temperature for 90 minutes, and the final concentration of YOYO-1 was 40 nM.

The buffer concentrations were 300 mM KCl and 20 mM Tris for all *previous data*, while it was 300 mM KCl, 20 mM Tris and 10 mM $MgCl_2$ for all measurements in *new results*. Again, the $MgCl_2$ was added as condensation by H-NS was not observed without it.

The spermine concentrations of interest were hard to determine, as low amounts could be added before aggregation occurred, compared to the concentrations used in FS. Initially, a range from 0-300 $\mu\mathrm{M}$ was investigated, but the ACF and images of the samples revealed that severe aggregation seemed to start between 0.5-1.0 $\mu\mathrm{M}$ spermine.

H-NS concentrations were not unproblematic to determine either, as little to no compaction was observed in the absence of crowding. Ultimately, concentrations between 0-2 $\mu\mathrm{M}$ H-NS worked well with crowding present, and seemed to include the most interesting regions

before aggregation occured.

The PEG concentrations were, as with FS, initially varied from 0-200 mg/ml, although the region between 0-60 mg/ml turned out to be the most interesting regions for FCS with H-NS, as the higher concentrations tended to induce aggregation.

3.3.3 Atomic Force microscopy

10 µl samples of the same composition as in FCS were loaded onto a freshly cleaved mica surface and incubated for 45 s. They were then rinsed in water and dried gently with compressed nitrogen, before being dried in a vacuum chamber overnight.

3.3.4 Electrophoresis Mobility Shift Assays

Final sample sizes were 10 µl, of same composition as with FCS, except from 5 $\mathrm{ng}/\mu\mathrm{l}$ DNA, to enhance image quality. The gels were post-stained overnight with $1\times$ GelRed dye.

Mixing Sequence

The mixing sequence used in FS, FCS, EMSAs and AFM is as follows:

1. MQ H_2O
2. Tris/KCl Mix ($MgCl_2$ included in experiments with H-NS)
3. Stained DNA
4. Condensing agent, either spermine or H-NS.
5. Incubate at room temperature for 30 minutes in darkness
6. Crowding agent, either PEG or BSA
7. Incubate at room temperature for 30 minutes in darkness

3.4 Instrumental Setup

There are numerous steps and instruments required on the path from a frozen bacterial culture to the measurement of stained, purified, linear plasmid. Freezers, fridges, burners, petri dishes, shaking incubators, water bath incubators, microwaves, scales, magnetic stirrers and centrifuges are just some of the tools utilized that will not be specified by brand and model, under the assumption of relatively invariable performance.

3.4.1 Concentration Measurement

Thermo Scientific NanoDrop ND-1000 Spectrophotometer was used for concentration measurement of DNA samples. It scans the absorption of the sample to provide an approximation of the concentration and purity of samples of about 1 µl in size. The data is represented in the form of an absorption spectra, and displays three key values; estimated concentration based on volume under the curve, and the key 260/230 and 260/280 ratios, which simply means the absorbance at 260 divided by that of 230 and 280. Since proteins

typically absorbs around 230, a low 260/230 ratio indicates protein contamination of the DNA sample.

3.4.2 Gel Electrophoresis

For gel electrophoresis, a 0.8% agarose gel with GelStar or GelRed dye was used. The voltage supply was a Bio-Rad PowerPack™ Basic Power Supply set at 100 V, and the gel was photographed using a Bio-Rad GelDoc™ with Bio-Rad Universal Hood II.

Electrophoresis Mobility Shift Assays

In contrast with normal gel electrophoresis, EMSAs were conducted using a loading dye without SDS, and an unstained 0.8% agarose gel. This was to minimize protein denaturation. In addition, the gel was run at 4 °C to ensure a more consistent binding activity.

3.4.3 Fluorescence Spectroscopy

The instrument used for FS was a Tecan Infinite® M200 PRO. It is capable of scanning a wide emission spectra of all wells on a plate of 96 samples consecutively. Multiple scans were done per well, in order to establish an error estimate of the inhomogeneity arising from dust or bubbles in the sample. Two formats of FS data were recorded for each well, one absolute value of the average emission at the wavelength of interest, and an emission scan from 520-700 nm, as shown in Figure 3.4. For Gelstar, the excitation and emission wavelengths were 493 and 540 nm, while for GFP was 485 and 525 nm.

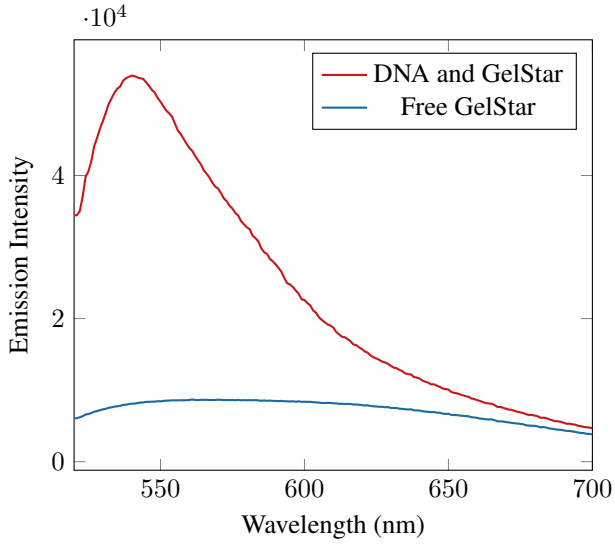

Figure 3.4: The emission spectrum free and DNA-bound GelStar. The DNA concentration is 2 ng/µl, and excitation wavelength is 493 nm.

3.4.4 Expression Assays

The samples were prepared according to the product protocol [83], but scaled down to a final sample volume of 25 µl. The T7 Master Mix is of a deep red color, which influences fluorescence spectroscopy as it has a baseline fluorescence emission spectrum, shown in Figure 3.5. To optimize the fluorescence measurement, the 25 µl sample was diluted to a 200 µl volume after incubation. This reduced the amount of bubbles in the sample, and made the red mixture less dense, reducing the absorbance of the GFP emission. A control with and without DNA is shown in Figure 3.5, showing the significant paseline emission spectrum of the T7 Master Mix.

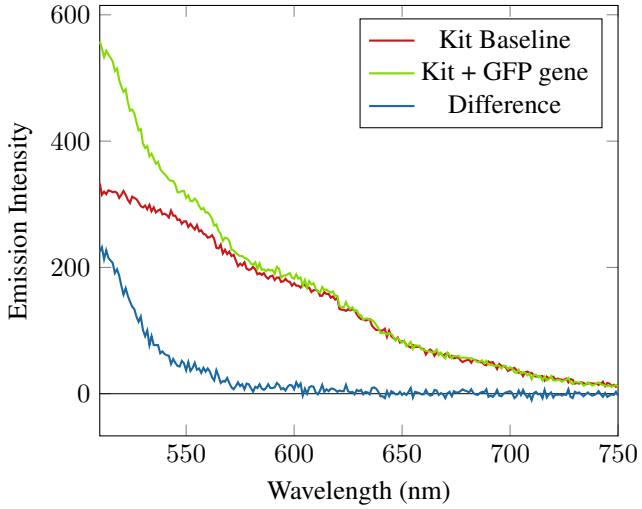

Figure 3.5: The emission spectra of the T7 Quick Master Mix with and without DNA, at 485 nm excitation wavelength.

3.4.5 Fluorescence Correlation Spectroscopy

The CLSM used for FCS was an inverted Leica SP8 with a 0.63x water immersion objective. Two argon excitation lasers were used, 514 nm for R6G, and 488 nm for YOYO-1 and Alexa-488, both with corresponding cleaning filters. The external detectors are from PicoQuant, and both were controlled by computer via the producer-developed softwares, Leica Application Suite X for microscope control and imaging, and SymphoTime for FCS data acquisition and processing. A simple illustration of the setup is shown in Figure 3.6. The water immersion lens is very sensitive to variations in the thickness and refractive index of the glass slides and samples, which can deteriorate the point-spread-function of the objective. To correct for this, the objective has a correction collar adjustment option, which axially moves the central lens group to restore optimal resolution and brightness [84]. The detector used for imaging was an internal photo multiplier tube (PMT) with variable absorption range. The detector used in all FCS measurements was an external

single-photon avalanche diode (SPAD), capable of singe-photon detection from the sample emission.

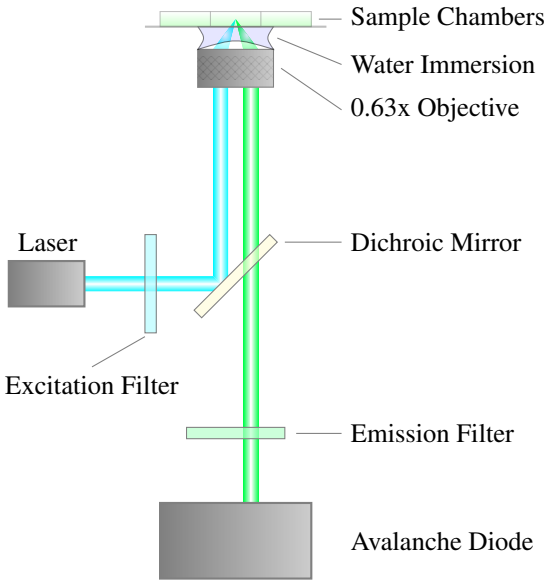

Figure 3.6: Illustration of the main components and light paths of the CLSM used for FCS. Illustration drawn with TikZ.

A lot of time went into finding the right measurement protocol. Longer recordings were prone to dust, shorter recordings were poor data for curve fitting. For FCS, a minimum of 6 recordings with a duration of 90 seconds were executed, with $\kappa = z_0/w_0 = 6.0$ for R6G and $\kappa = z_0/w_0 = 4.0$ for DNA. The difference in κ is due to the different size of the particles. This protocol, combined with the use of weighted arithmetic means for data analysis gave a lower error, without much subjective influence on the results. The effective focal volume was set to the default 1 fl during curve fitting, as normalized data were sufficient. The curve-fitting algorithm tends to give a high triplet-state relaxation time, often above 40 ns, and had to be adjusted manually to a more realistic number, closer to 10 ns.

Chapter 4

Results

Because the results from the preparatory project were acquired using a slightly different buffer, different DNA stock, and an older FCS protocol, the two are separated to avoid confusion.

4.1 Previous Data

Some previous data on the project is worth discussing, mainly the FS and FCS work done on DNA with PEG and spermine. Note that these experiments were conducted with the 6010 bp pSB-M2g-1-17 plasmid, without $MgCl_2$ in the buffer, that spermine concentrations are reported in spermine/DNA-bp ratio, and that all data were normalized.

4.1.1 Dye Exclusion Induced by PEG

The results of dye exclusion assay upon the addition of PEG are shown in Figure 4.1. A reduction in fluorescence is clearly visible in higher PEG concentrations.

4.1.2 Dye Exclusion Induced by Spermine

The first set of dye exclusion experiments with addition of spermine are displayed in Figure 4.2. The data could indicate that the intensity actually rises with lower concentrations of spermine. This lower region was investigated further by a set of measurements at lower concentrations, shown in Figure 4.3. Although high standard deviations render this result insignificant, a slight increase can be indicated between $C_{\mathrm{spm}}/C_{\mathrm{DNA-bp}} = 0 \rightarrow 2.5$.

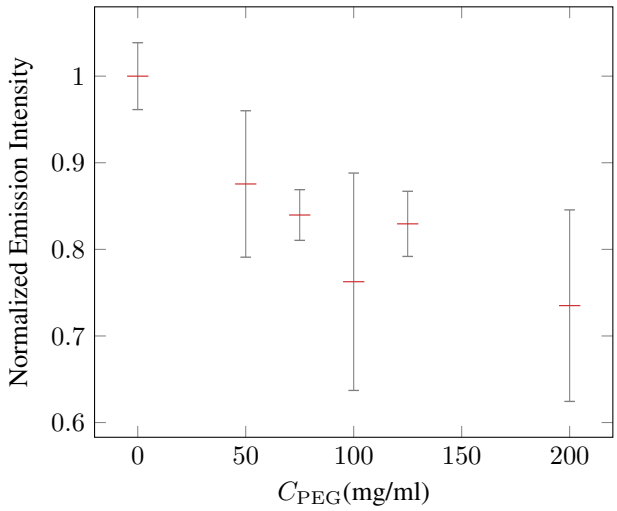

Figure 4.1: Normalized fluorescence intensity of DNA-GelStar complexes, shown as a function of PEG concentration C_{PEG}. Concentration of DNA is 2 $\mathrm{ng}/\mu\mathrm{l}$, and excitation and emission wavelengths were 493 and 527 nm, respectively.

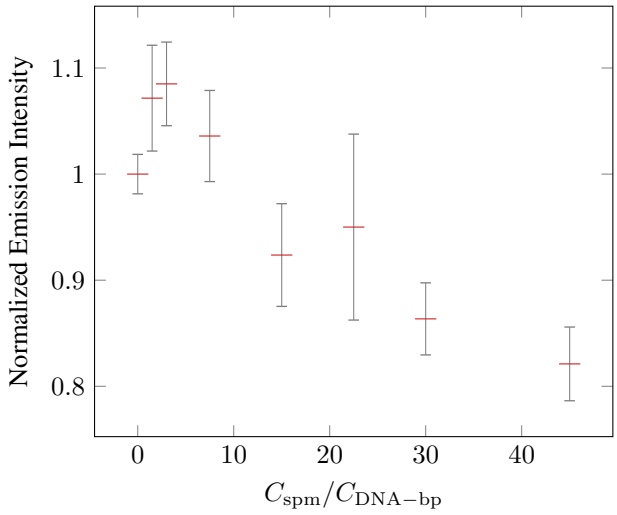

Figure 4.2: Normalized fluorescence intensity of DNA-GelStar complexes, shown as a function of $C_{\mathrm{spm}}/C_{\mathrm{DNA-bp}}$. Concentration of DNA is 2 $\mathrm{ng}/\mu\mathrm{l}$, and excitation and emission wavelengths were 493 and 527 nm, respectively.

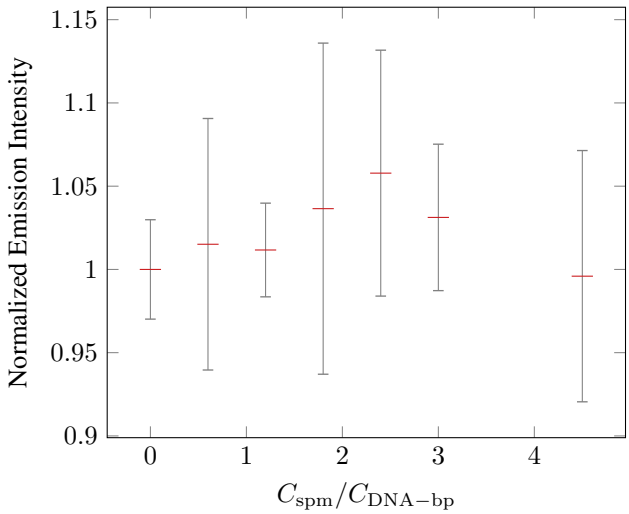

Figure 4.3: Normalized fluorescence intensity of DNA-GelStar complexes, shown as a function of $C_{\mathrm{spm}}/C_{\mathrm{DNA-bp}}$. Concentration of DNA is 2 $\mathrm{ng}/\mu\mathrm{l}$, and excitation and emission wavelengths were 493 and 527 nm, respectively.

4.1.3 Effect of PEG on Viscosity and DNA Diffusion

Diffusion of the 6010 bp pSB-M2g-1-17 plasmid upon addition of 0, 100 and 200 mg/ml PEG are available as the initial values at $C_{\mathrm{spm}}/C_{\mathrm{DNA-bp}} = 0$ in the FCS results in Figure 4.7. The results are for clarity also displayed in Figure 4.4. In order to estimate whether or not DNA condensation is taking place under the addition of PEG, a measurement of the change in viscosity is needed. The relative viscosities η/η_0 of the PEG concentrations in Figure 4.4 were measured with R6G, shown in Table 4.1.

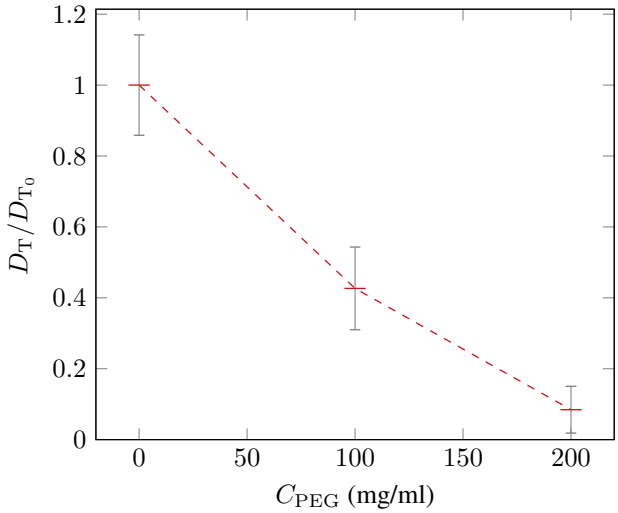

Figure 4.4: Relative change in D_{T} of linearized plasmid pSB-M2g-1-17 DNA-YOYO-1 complexes with varying PEG concentration, where $D_{\mathrm{T_0}}$ is the translational diffusion coefficient of the DNA-YOYO-1 complex in the absence of PEG. Final DNA concentration id 2 $\mathrm{ng}/\mu\mathrm{l}$. Dashed lines are guides to the eye.

Table 4.1: Relative viscosities η/η_0 of the PEG solutions used for experiments with spermine and PEG, as estimated by diffusion coefficients of R6G. η_0 is the viscosity with no PEG added.

PEG Concentration mg/ml	Viscosity η/η_0	SD $\Delta\eta/\eta_0$
0	1.00	$\pm$0.07
100	3.81	$\pm$0.33
200	6.77	$\pm$0.58

4.1.4 Effects of Spermine on DNA Diffusion

The initial experiments were done to find the concentration region of interest for spermine, starting with $C_{\mathrm{spm}}/C_{\mathrm{DNA-bp}} = 0 \rightarrow 150$. This gave highly inconsistent results, and flu-

orescence microscope images of the samples, some of which are shown in Figure 4.5, revealed extensive aggregate formation at even the lowest concentrations, indicating that these concentrations were too high for single molecule investigation. By this, we quickly learned how sensitive FCS is to aggregation.

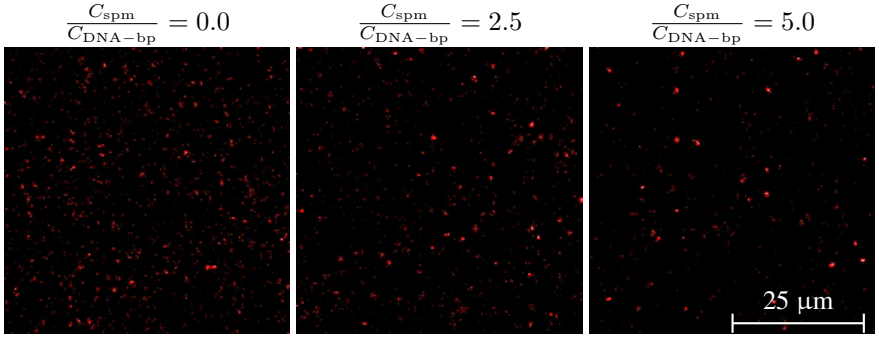

Figure 4.5: Images of the aggregation which occured during the first titration of spermine vs the linear pSB-M2g-1-17 plasmid.

The next titration was $C_{\mathrm{spm}}/C_{\mathrm{DNA-bp}} = 0 \rightarrow 3$, shown in Figure 4.6. Here, we see an increase in the relative translational diffusion of DNA followed by a decrease for $C_{\mathrm{spm}}/C_{\mathrm{DNA-bp}} \geq 1$, which could indicate that the condensation and consecutive aggregation all starts to happen within this regime. This regime was then chosen for the experiments with both spermine and PEG, in Section 4.1.5.

4.1.5 Combined DNA Condensation by PEG and Spermine

When the PEG and spermine concentration ranges of interest were established, the combination was examined. The concentrations of PEG were set to 0, 100 and 200 mg/ml. The spermine concentrations were $C_{\mathrm{spm}}/C_{\mathrm{DNA-bp}} = 0 \rightarrow 1$ with 0.125 step width. The results are shown in Figure 4.7. The lower concentrations of PEG seem to reveal some condensation before $C_{\mathrm{spm}}/C_{\mathrm{DNA-bp}} = 1$, which was to be expected. Fluorescence micrographs were acquired for each sample, some of which are shown in Figure 4.8.

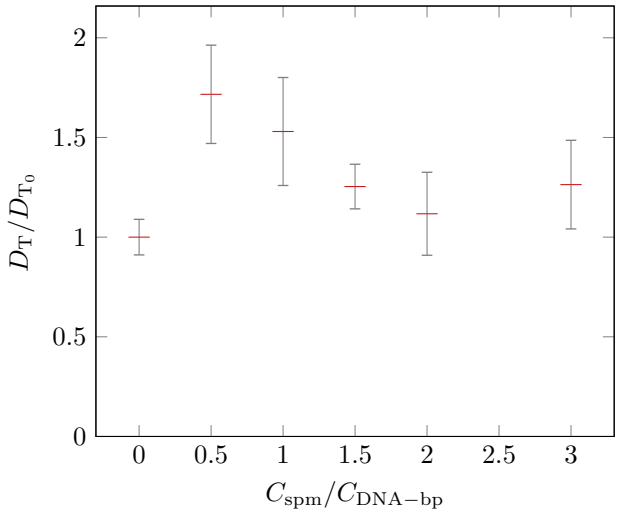

Figure 4.6: Relative change in D_T of linearized plasmid pSB-M2g-1-17 DNA-YOYO-1 complexes with varying spermine to DNA-bp concentration ratio, where D_{T_0} is the translational diffusion coefficient of the DNA-YOYO-1 complex in the absence of both PEG and spermine. Final DNA concentration is 2.25 $\mathrm{ng}/\mu\mathrm{l}$.

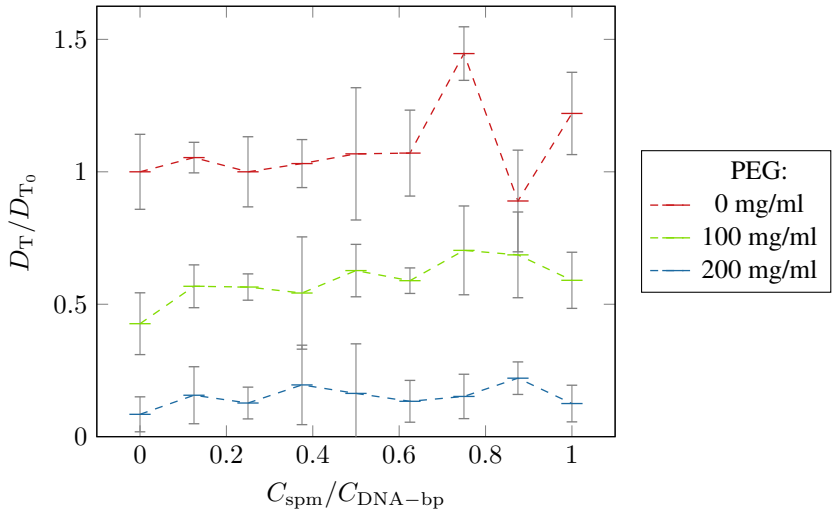

Figure 4.7: Relative change in D_T of linearized plasmid pSB-M2g-1-17 DNA-YOYO-1 complexes varying with C_{spm}/C_{DNA-bp} and PEG concentration, where D_{T_0} is the translational diffusion coefficient of the DNA-YOYO-1 complex in the absence of both PEG and spermine. Final DNA concentration 2 $\mathrm{ng}/\mu\mathrm{l}$. Dashed lines are guides to the eyes.

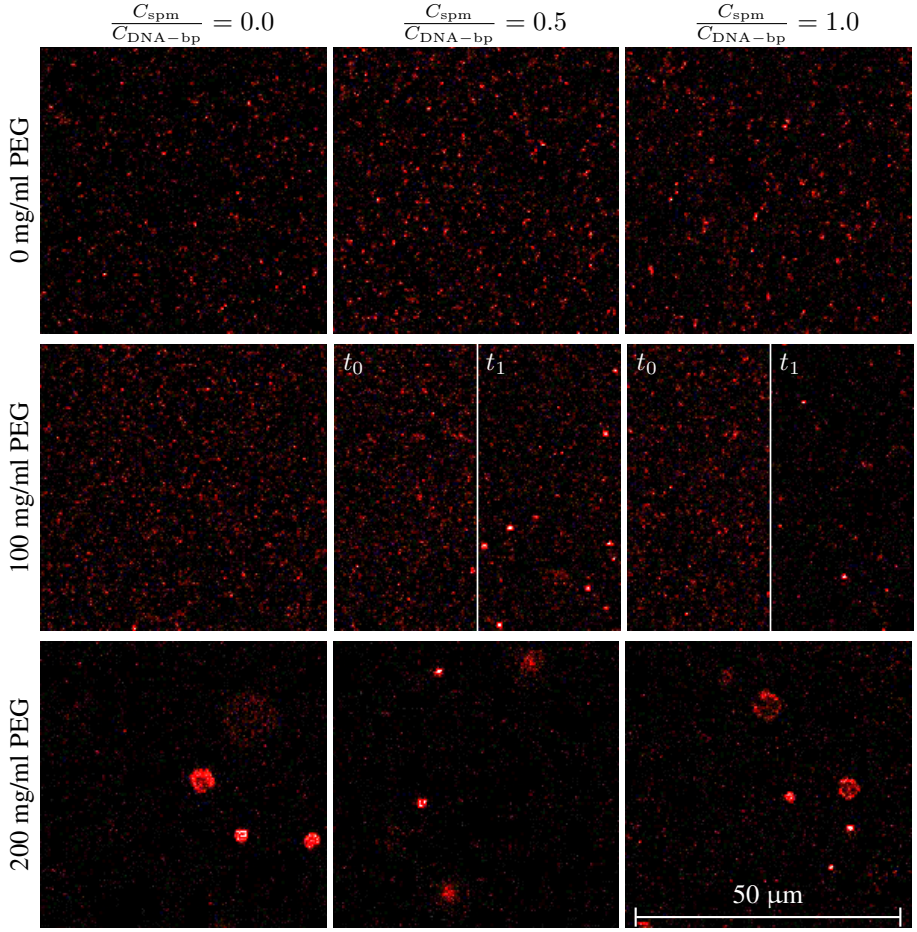

Figure 4.8: An image set of the diffusing complexes at 0, 100 and 200 mg/ml PEG, and 0, 0.5 and 1.0 $C_{\mathrm{spm}}/C_{\mathrm{DNA-bp}}$ ratio, respectively. Images labeled t_0 and t_1 indicates capture before and after measurement, respectively. All other images were captured before the FCS measurement.

4.2 New Results

In the new results, diffusion coefficients are initially given in absolute values. This is because with the new FCS protocol, the focal volume was found to be close to the software default of 1 fl, as discussed in Section 4.2.2. This way, one can get an impression of the real sizes and speeds of the system.

4.2.1 Dye Exclusion by H-NS

A substantial effort was put into quantifying the dye exclusion by H-NS, but surprisingly, there was no significant reduction in emission upon addition of even the highest concentrations of the protein, and in fact rather showed an increase in fluorescence. Even in the presence of PEG, the addition of H-NS did not reduce emission. This led to the hypothesis that H-NS does not collapse the DNA tight enough to have significant effect on the availability of the DNA strands, that the GelStar dye interacts with H-NS, or a combination. A control without DNA confirmed the protein-dye interaction, but did not give any information on the exclusion.

4.2.2 FCS Optimization and Preparation

The protocol used in the old data gave high deviations and little significance in the results, so measures were taken to optimize this protocol. Initially, R6G was used to standardize the FCS protocol, including inspecting the afterpulse duration and lag-time region of interest. The ACFs of three consecutive 90 s measurements are shown in Figure 4.9. These results give a mean of 449.2 $\pm$ 7.8 $\mu m^2/s$, a relative standard deviation of less than 1.8%. The true experimental diffusion coefficient for this has been shown to be 414-430 $\mu m^2/s$ [85], indicating that our focal volume is a bit smaller than the default 1 fl, but within close proximity. The ACFs of three consecutive 90 s measurements with 4017 bp PCR product are shown in Figure 4.10. This yielded a mean value of 7.44 $\pm$ 0.23 $\mu m^2/s$, a relative standard deviation of 3.1%. The comparison of these graphs make it evident that the measurement protocol is satisfactory and, the error is within a reasonable range, compared to the old FCS results. Figure 4.10 shows only three ACFs, but a minimum of six were used in all new data.

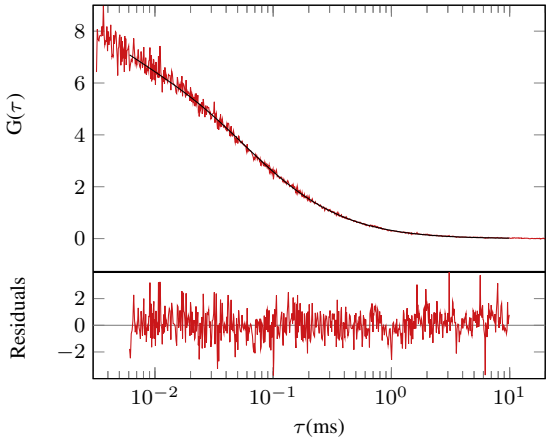

$D_{\mathrm{T}}(\mu\mathrm{m}^2/\mathrm{s})$	$=439.79$	± 5.44
$\langle N \rangle$	$=0.134$	± 0.021
$\langle C \rangle(\mathrm{nM})$	$=0.222$	± 0.035
T	$=0.2037$	± 0.0883
$\tau_{\mathrm{T}}(\mathrm{ms})$	$=0.004$	
$\kappa = z_0/w_0$	$=6.0$	
$V_{\mathrm{Eff}}(\mathrm{fl})$	$=1.0$	

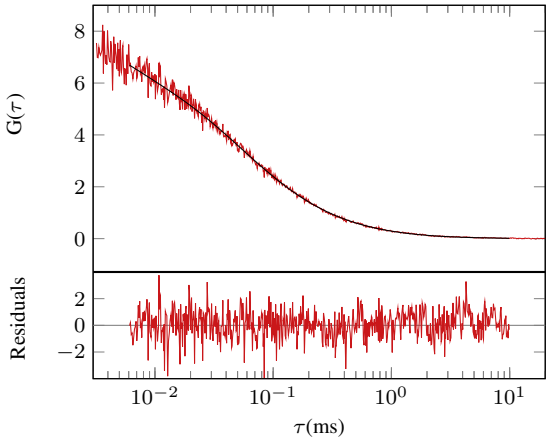

$D_{\mathrm{T}}(\mu\mathrm{m}^2/\mathrm{s})$	$=453.87$	± 7.16
$\langle N \rangle$	$=0.141$	± 0.015
$\langle C \rangle(\mathrm{nM})$	$=0.234$	± 0.026
T	$=0.1996$	± 0.0703
$\tau_{\mathrm{T}}(\mathrm{ms})$	$=0.004$	
$\kappa = z_0/w_0$	$=6.0$	
$V_{\mathrm{Eff}}(\mathrm{fl})$	$=1.0$	

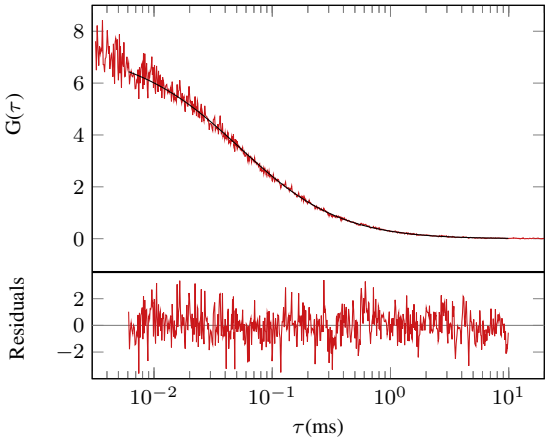

$D_{\mathrm{T}}(\mu\mathrm{m}^2/\mathrm{s})$	$=457.31$	± 7.59
$\langle N \rangle$	$=0.140$	± 0.016
$\langle C \rangle(\mathrm{nM})$	$=0.232$	± 0.027
T	$=0.0.314$	± 0.0761
$\tau_{\mathrm{T}}(\mathrm{ms})$	$=0.004$	
$\kappa = z_0/w_0$	$=6.0$	
$V_{\mathrm{Eff}}(\mathrm{fl})$	$=1.0$	

Figure 4.9: ACF and fitted curve from three 90 second FCS measurements of 8 nM R6G.

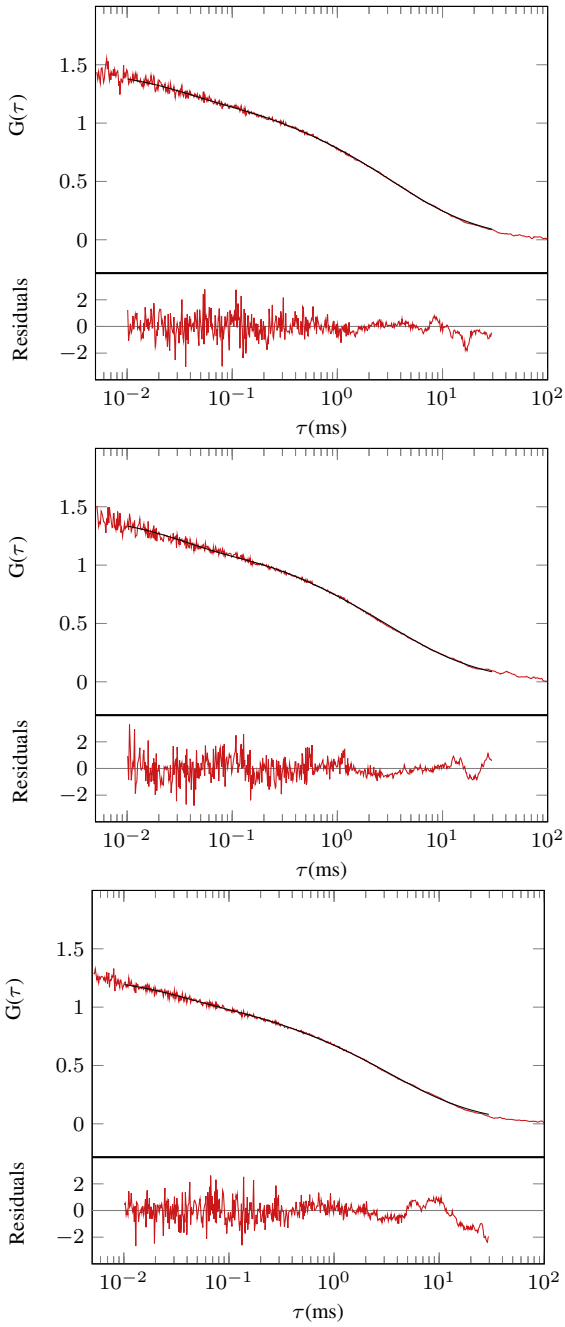

$D_{T_1}(\mu m^2/s)$	$=7.681$	± 0.177
$D_{T_2}(\mu m^2/s)$	$=106.5$	± 13.8
$\langle N \rangle$	$=0.804$	± 0.016
$\langle C \rangle$(nM)	$=1.336$	± 0.027
T	$=0.145$	± 0.013
τ_T(ms)	$=0.010$	
$\kappa = z_0/w_0$	$=4.0$	
V_{Eff}(fl)	$=1.0$	

$D_{T_1}(\mu m^2/s)$	$=7.092$	± 0.293
$D_{T_2}(\mu m^2/s)$	$=66.9$	± 10.3
$\langle N \rangle$	$=0.866$	± 0.034
$\langle C \rangle$(nM)	$=1.437$	± 0.057
T	$=0.188$	± 0.018
τ_T(ms)	$=0.010$	
$\kappa = z_0/w_0$	$=4.0$	
V_{Eff}(fl)	$=1.0$	

$D_{T_1}(\mu m^2/s)$	$=7.405$	± 0.190
$D_{T_2}(\mu m^2/s)$	$=113.6$	± 19.6
$\langle N \rangle$	$=0.929$	± 0.022
$\langle C \rangle$(nM)	$=1.542$	± 0.037
T	$=0.145$	± 0.017
τ_T(ms)	$=0.010$	
$\kappa = z_0/w_0$	$=4.0$	
V_{Eff}(fl)	$=1.0$	

Figure 4.10: ACF and fitted curve from three 90 second FCS measurements of 2.25 $ng/\mu l$ 4017 bp PCR product in solution.

4.2.3 Effects of PEG and BSA on Viscosity and DNA Diffusion

PEG

The diffusion of the 4017 bp PCR product upon addition of 0, 20, 40 and 60 mg/ml is shown as initial values, at 0 μM H-NS in Figure 4.16, for clarity also displayed in Figure 4.11. The relative viscosities η/η_0 of the PEG concentrations in this experiment were measured with R6G, shown in Table 4.2.

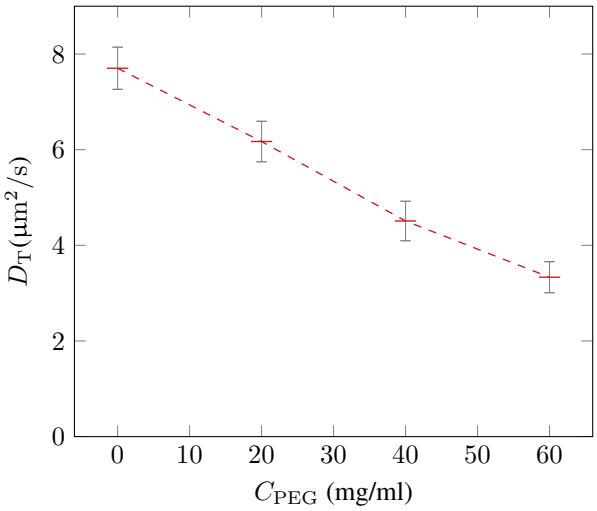

Figure 4.11: Translational diffusion coefficient D_T of 4017 bp PCR product with varying PEG concentration. Final concentration of DNA is 2.25 $ng/\mu l$. Dashed lines are guides to the eye.

Table 4.2: Relative viscosity η/η_0 of the solutions of PEG used in experiments with PEG and H-NS, as measured by the diffusion of R6G. η_0 is the viscosity with no PEG added.

PEG Concentration mg/ml	Viscosity η/η_0	SD $\Delta\eta/\eta_0$
0	1.00	±0.01
20	1.43	±0.02
40	1.66	±0.05
60	2.08	±0.06

BSA

The effects of BSA concentrations are shown in Figure 4.17, where it seems that 2.5% has little impact on the initial diffusion coefficients. 5% on the other hand, shows significant

decrease, similar to that of 6% PEG. This is interesting, as both seem to comparable impacts on viscosity at the same mass concentrations.

Substantial efforts were made to quantify the viscosity of BSA solutions. Firstly, as with PEG, the viscosity was measured with R6G, with confusing results, The diffusion constant of R6G fell from a seemingly single species at $\simeq 450\ \mu\mathrm{m}^2/\mathrm{s}$ to a polydisperse population with a mean diffusion coefficient well under 20 $\mu\mathrm{m}^2/\mathrm{s}$ at 2.5% BSA, which seemed to be a big drop just due to the viscosity change. Further research revealed that BSA as a carrier protein binds to the R6G [86], thus making this a measurement of the diffusion of BSA, rather than R6G alone. In an effort to solve this, R6G-BSA complexes were incubated, and an 8 nM concentration of these was added to the 0, 2.5 and 5% BSA solutions, to use the BSA as a reference instead of free R6G. This gave poor results, as the dye partly dissociates, and because the fluorescence of 2.5% BSA is higher than that of nM concentrations of R6G by a long shot, at the excitation and emission wavelengths suited for this fluorophore. An effort was made to measure by a capillary viscometer, but foaming and bubbling of the BSA made this approach futile. Papers on viscosity of BSA solutions are many [87][88], but these are mostly on lower concentrations, or with salt conditions not comparable to our setup.

4.2.4 Confirming H-NS Binding Activity

After purification of the protein and identification by mass spectroscopy, several tests were conducted to confirm that it was in fact active. As mentioned, the protein increases fluorescence of GelStar and YOYO-1, which made these nucleotide probes unfit for both FS and FCS, as the diffusion of now fluorescent oligomers of protein was hard to distinguish from DNA. Subsequently, gel mobility shift assays were conducted, the first of which shown in Figure 4.12, showing clear reduction in mobility from 5-10 $\mu\mathrm{M}$ H-NS. To investigate the binding of H-NS more closely, AFM was used to image DNA with and without 5 $\mu\mathrm{M}$ H-NS, shown in Figure 4.13. Here, aggregation is visible, indicating that 5 $\mu\mathrm{M}$ H-NS could be too high a concentration for single-molecule investigation by FCS. The binding was also investigated with a cell-free expression assay, shown in Figure 4.14, where significant inhibition of GFP expression is shown at concentrations as low as 0.1 $\mu\mathrm{M}$ H-NS.

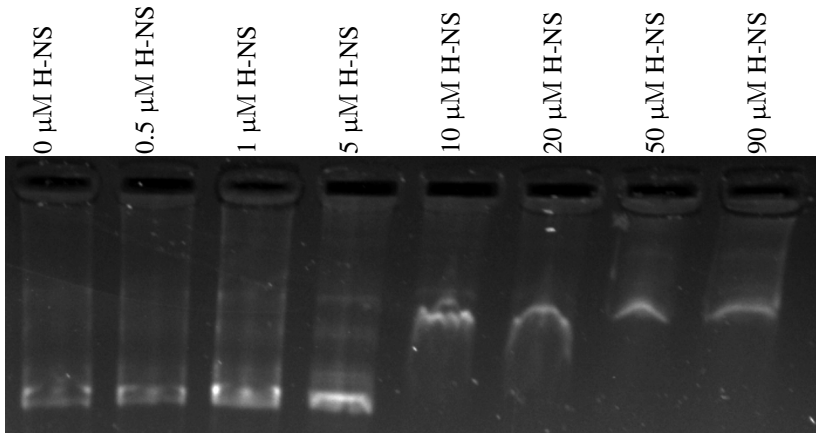

Figure 4.12: Gel shift assay of 4017 bp PCR product under the influence of 0-100 μM H-NS. Sample sizes were 10 μl and DNA concentration was 5 $\mathrm{ng}/\mu\mathrm{l}$.

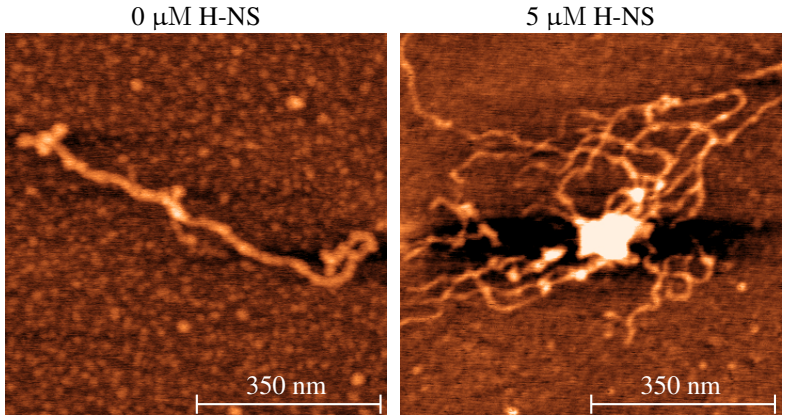

Figure 4.13: AFM micrographs of 4017 bp PCR product under the influence of 0 and 5 μM H-NS, indicating aggregation in the higher concentrations. The final concentration of DNA is 2.25 $\mathrm{ng}/\mu\mathrm{l}$.

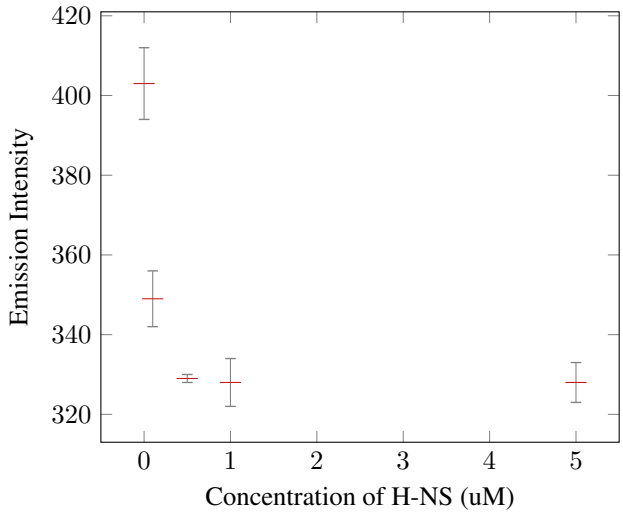

Figure 4.14: Emission intensity from GFP expression samples at different concentrations of H-NS. Final DNA concentration is 3.6 $\mathrm{ng}/\mu\mathrm{l}$, and excitation and emission wavelengths were 485 and 525 nm respectively.

4.2.5 DNA Condensation by H-NS

It turned out to be hard to quantify the change in diffusion of DNA during the addition of H-NS by FCS. The main observation seemed to be a significant increase in deviations between the measurements of the same sample at higher concentrations of H-NS, and little to no increase in diffusion. This result persisted through several replicas, until crowding agents were added as a test. The first breakthrough with FCS was achieved upon the addition of 40 mg/ml PEG, and this set is shown in Figure 4.15. A set with 0% PEG was also conducted in this investigation, and a slight increase in diffusion can be observed here too, but this turned out to be more of an exception than the general result. An additional FCS investigation of diffusion at 0, 2, 4 and 6% PEG is shown in Figure 4.16, showing that the relative condensation is very much dependent on the crowding environment. In these measurements, care was also taken to detect aggregation in the sample, shown with crosses. The next FCS investigation was on the effect of BSA on H-NS-induced condensation, shown in Figure 4.17. Here an amount of condensation is apparent, and aggregation at 2.5 and 5% BSA is observed in the same concentration regions of H-NS as with 4 and 6% PEG.

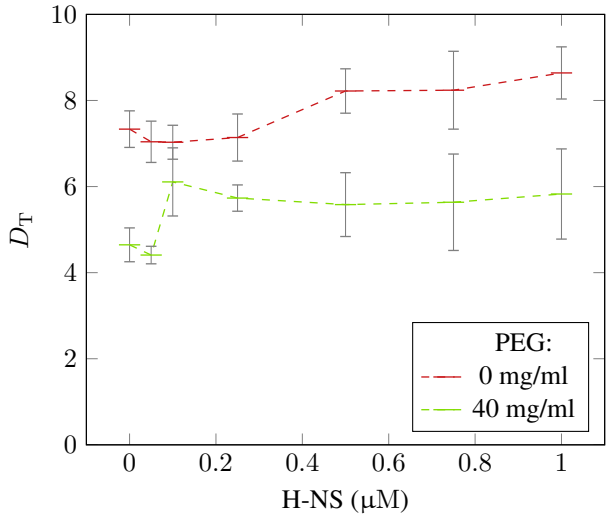

Figure 4.15: Diffusion coefficient of 2.25 $\mathrm{ng}/\mu\mathrm{l}$ 4017 bp PCR product at different concentrations of H-NS and PEG. Lines are guides to the eyes.

4.2.6 GFP Expression under influence of PEG and H-NS

The impact of PEG and H-NS on expression of GFP is shown in Figure 4.3. This investigation reveals some interesting effects of PEG and H-NS. Most apparent is that high concentrations of PEG and H-NS inhibit the expression of GFP. Furthermore, lower concentrations of H-NS, 0.05-0.1 $\mu\mathrm{M}$, could seem to aid in the expression in several of the

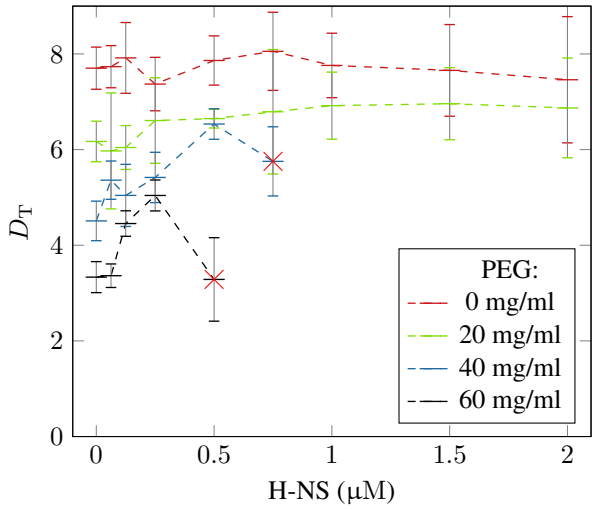

Figure 4.16: Diffusion coefficient of 2.25 ng/µl 4017 bp PCR product at different concentrations of H-NS and PEG. Red crosses indicate visual confirmation of aggregation, whereby the rest of the set is excluded from the graph. Lines are guides to the eyes.

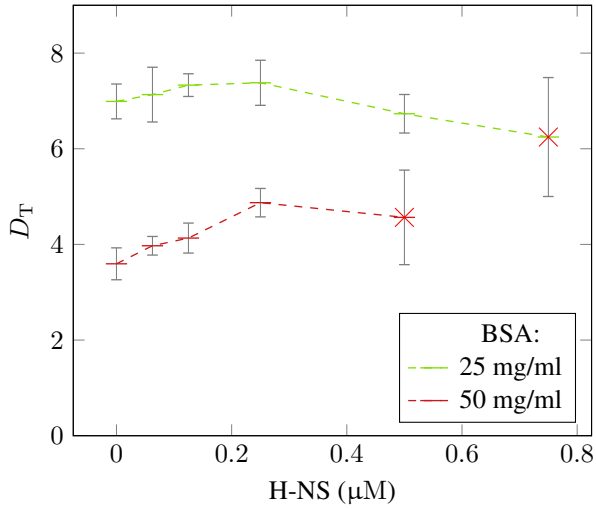

Figure 4.17: Diffusion coefficient of 2.25 ng/µl 4017 bp PCR product at different concentrations of H-NS and BSA. Red crosses indicate visual confirmation of aggregation, whereby the rest of the set is excluded from the graph. Lines are guides to the eyes.

rows, mostly at 1 and 2% PEG. The standard deviations naturally renders these observations inconclusive, but interesting nonetheless. To use BSA in the expression kit turned out to be a quite costly procedure, as the auto-fluorescence of BSA would make it necessary to keep blanks for every concentration.

Table 4.3: Normalized emission intensity from GFP expression samples at different concentrations of H-NS and PEG. Final DNA concentration is 3.6 ng/µl of 4016 bp PCR product, and excitation and emission wavelengths were 485 nm and 525 nm, respectively.

	0% PEG	0.5% PEG	1% PEG	2% PEG	4% PEG
HNS (µM)	Emission Intensity				
0.00	1.00 ± 0.04	0.83 ± 0.15	0.66 ± 0.15	0.21 ± 0.06	0.11 ± 0.11
0.05	1.02 ± 0.13	0.85 ± 0.17	0.68 ± 0.15	0.21 ± 0.06	0.00 ± 0.09
0.10	1.02 ± 0.13	0.64 ± 0.09	0.68 ± 0.13	0.30 ± 0.09	0.02 ± 0.06
0.25	0.77 ± 0.13	0.77 ± 0.09	0.72 ± 0.19	0.38 ± 0.09	0.09 ± 0.09
0.50	0.36 ± 0.11	0.49 ± 0.04	0.66 ± 0.53	0.17 ± 0.17	0.06 ± 0.09
0.75	0.32 ± 0.09	0.15 ± 0.21	0.26 ± 0.04	0.17 ± 0.06	0.04 ± 0.02
1.00	0.13 ± 0.09	0.26 ± 0.06	0.17 ± 0.11	0.09 ± 0.11	0.15 ± 0.11

4.2.7 Electrophoresis Mobility Shift Assays

As expression assays seemed unfit for investigation of the effects of BSA, binding assays were conducted with both BSA and PEG, to get a better picture of the effects in play during condenstation, the first of which shown in Figure 4.18. Here, both 2-6% PEG and 2.5-5% BSA are shown to significantly assist in the binding of H-NS. Most impressive is the BSA, which yields a very defined band, in addition to the highest mobility decrease. A second mobility shift was conducted with a BSA control, in case it induced mobility shift also in the absence of H-NS. This assay is shown in Figure 4.19, revealing that the mobility reduction due to BSA alone is far from as effective as in combination with H-NS. A reduction in band intensity is visible, which could be due to some yet unclear interaction between BSA and DNA. The 5 µM concentration of H-NS was chosen as it seemed to be close to the transition concentration in the gel shift assay in Figure 4.12.

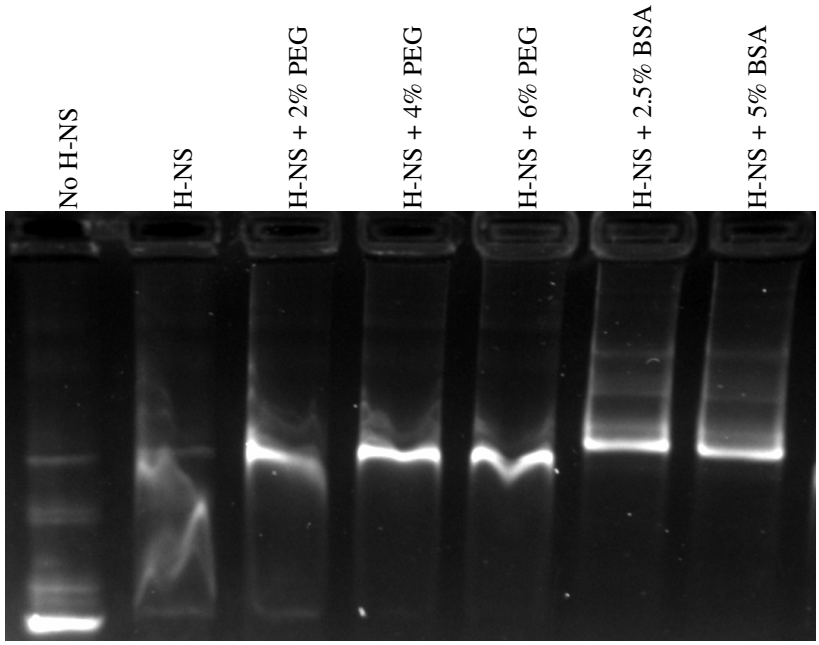

Figure 4.18: Gel shift assay of 4017 bp PCR product under the influence of 5 μM H-NS, with PEG and BSA. Sample sizes were 10 μl and DNA concentration was 5 $\mathrm{ng}/\mu\mathrm{l}$.

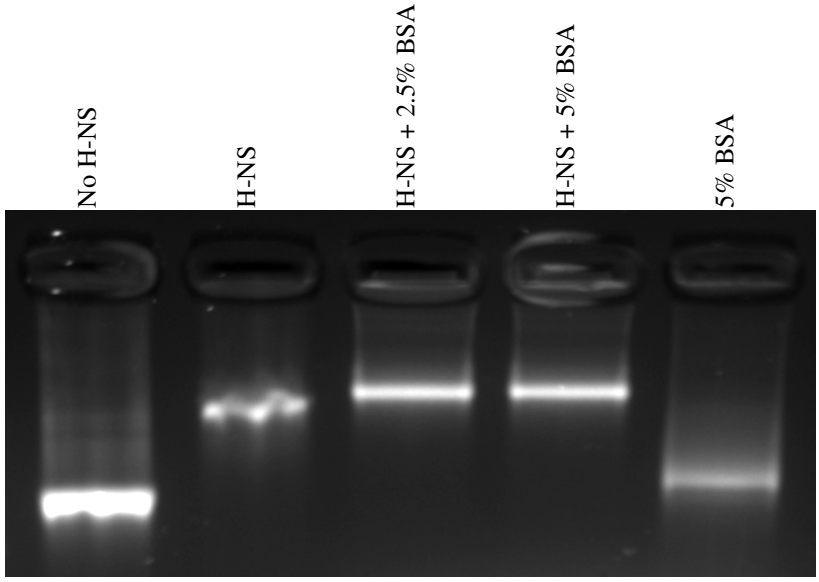

Figure 4.19: Gel shift assay of 4017 bp PCR product under the influence of 5 μM H-NS and BSA. Sample sizes were 10 μl and DNA concentration was 5 $\mathrm{ng}/\mu\mathrm{l}$.

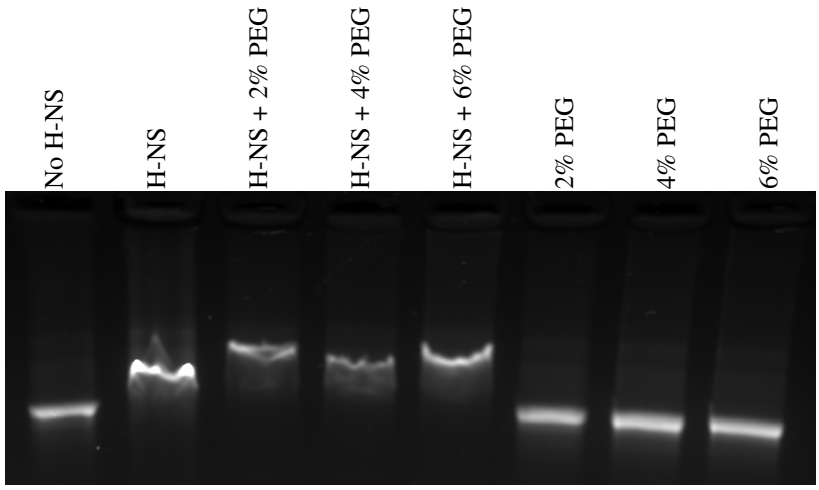

Figure 4.20: Gel shift assay of 4017 bp PCR product under the influence of 5 μM H-NS and PEG. Sample sizes were 10 μl and DNA concentration was 5 $\mathrm{ng}/\mu\mathrm{l}$.

Chapter 5

Calculations and Discussion

5.1 Previous Data

5.1.1 Dye Exclusion By PEG

The results from dye exclusion, shown in Figure 4.1, clearly show significant decrease in emission intensity upon increase in PEG concentration. This indicates that the DNA is less accessible to GelStar, and thus, has assumed a more compact conformation. This is in agreement with the results from FCS.

5.1.2 DNA Condensation by PEG

The condensation by PEG can be investigated by using the data shown in Figure 4.4 and applying the viscosity correction data from Table 4.1, to achieve the corrected values shown in Figure 5.1. It is apparent from this figure that condensation is occurring at 100 mg/ml PEG, while aggregation seems to have occured at 200 mg/ml PEG, as confirmed by the image set shown in Figure 4.8.

5.1.3 Dye Exclusion By Spermine

The spermine concentration regime suitable for FCS was found to be much lower than what had been used in FS, due to aggregation. Furthermore, as shown in Figure 4.2, there seems to be an increase in bound dye between $C_{\mathrm{spm}} \,/\, C_{\mathrm{DNA-bp}} = 0 \rightarrow 1.2$, which could be perceived as contradictory to what one might expect. Although the error margins are a bit too large to ensure confidence, the results in Figure 4.3 reinforce the notion that there is a slight increase in emission intensity at lower concentrations. Further research would be required in order to identify the etiology of this increase in emission.

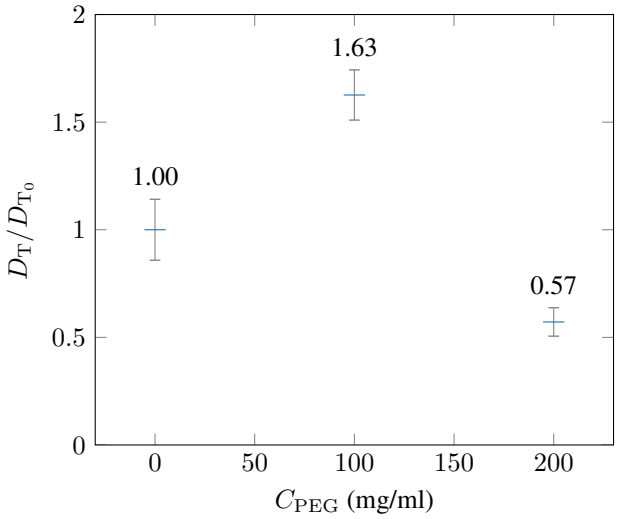

Figure 5.1: Relative change in D_T of linearized plasmid pSB-M2g-1-17 DNA-YOYO-1 complexes with varying PEG concentration.

5.1.4 DNA Condensation By Spermine

The results of condensation by spermine alone is shown in Figure 4.6. Naturally, the diffusion coefficient increases, and seems to drop around C_{spm} / C_{DNA-bp} 0.5 $\rightarrow$ 1, at what seems to be the threshold concentration before aggregation dominates the system. An increase and drop in the concentration region C_{spm} / C_{DNA-bp} 0 $\rightarrow$ 1 is in agreement with the data in Figure 4.7.

5.1.5 Combined DNA Condensation by PEG and Spermine

There are numerous curious observations in the results from the combination of PEG and spermine. Firstly, and most obvious from the visual evidence in Figure 4.8, is the local gathering of DNA upon the addition of 200 mg/ml PEG. This is in part due to the higher viscosity of the medium, in which brownian collisions will have reduced effect on dissociation, which would otherwise separate and disorder the complexes. A lower energy is here achieved by the two-phase separation between regions of DNA, dominated by electrostatic interactions, and phase constituted by the less charged PEG, creating a viscous surrounding, which together could be similar to cytoplasmic conditions in bacteria. The FCS data for 200 mg/ml PEG, shown in Figure 4.7 clearly shows a very low diffusion constant at all concentrations of spermine, consistent with the imaging. Some increase in diffusion can be observed from C_{spm} / $C_{DNA-bp} = 0.0 \rightarrow 0.875$, but since the number density of diffusing bodies is low, and there is significant polydispersity, the results are hardly more than indications. If there truly is an increase, it could be because condensed DNA allows for further compaction of the aggregate volumes.

Furthermore, from the visual evidence, a similar effect can be observed over time in the case of 100 mg/ml PEG in the presence of spermine concentrations higher than C_{spm} / $C_{\mathrm{DNA-bp}} \approx 0.5$. After mixing, the samples look dispersed, while after the FCS measurement of 6 minutes, local aggregates can be observed, indicating that the viscosity and crowding effects are limiting the dispersive effects of the brownian forces in this case as well. Therefore, an even higher D_{T} could be expected than the results indicate, as the sample could include dimers and oligomers of DNA-complexes some time after the measurement is started. From Figure 4.8, little can be concluded from the image set with 0 mg/ml PEG, other than that maybe some aggregation is visible in the case of $C_{\mathrm{spm}}/C_{\mathrm{DNA-bp}} = 1.0$, which is in agreement with the FCS data, where the diffusion constant seemingly begins to fluctuate significantly, indicating that aggregates are beginning to affect the measurement.

The standard deviations in these measurements are too high to give them much credit. But for sport, some calculations were performed. Taking the results from Figure 4.7, and applying the data acquired with R6G in Table 4.1, namely the relative change in diffusion of R6G according to PEG concentration, leads to the adjusted data in Figure 5.2. Now that the increase in viscosity is accounted for, two things are more evident, firstly the increase in diffusion at 100 mg/ml PEG is revealed, and secondly, the large decrease in diffusion upon 200 mg/ml PEG, along with the very high error makes it clearer that aggregation has occured. Excluding the set at 200 mg/ml PEG, the relative change in translational diffusion according to Equation 2.4 is shown in Figure 5.3. Here the difference is evident, and one can see that the combination of PEG and spermine achieves a 2.68-fold increase in diffusion.

To get an idea of the change in volume, one can assume the DNA complexes to be spherical in shape, and apply Equation 2.5. The results of this calculation is shown in Figure 5.4, after ignoring the values over the assumed limit of aggregation, $C_{\mathrm{spm}}/C_{\mathrm{DNA-bp}} \geq 0.875$. Here the inverse cubic relation between the diffusion and the volume makes it easier to appreciate the changes occurring in the sample. At the highest obtained diffusion without PEG, the volume is approximately ≈33% of the initial value, whereas the addition of PEG leads to a reduction of volume to ≈5%, which is similar to the compaction of genomic DNA found in *E.Coli*, which can be 2.5% of the unconstrained DNA volume under low ionic strength [6]. The ionic strength is substantial in this set of experiments ($\sim$ 300 mM), so the degree of compaction from low ionic conditions could be even higher than the compaction encountered here. Finally, one can see that the product of the compaction from PEG and spermine alone, $23\% \cdot 33\% \approx 7.6\%$ is not as efficient as the combination, which could point to a degree of synergism. Again, the error is too high to conclude anything, other than that it is very likely that some compaction has indeed been induced.

5.1.6 Comparison to Dye Exclusion Data

As mentioned, the suitable concentration regime of spermine for FCS was only a fraction of the concentrations used in FS, which complicates the comparison of data from both sources, and when it comes to the lower concentrations of spermine in FS, the data actually seem to indicate the opposite of FCS, but this could rather indicate that there is some

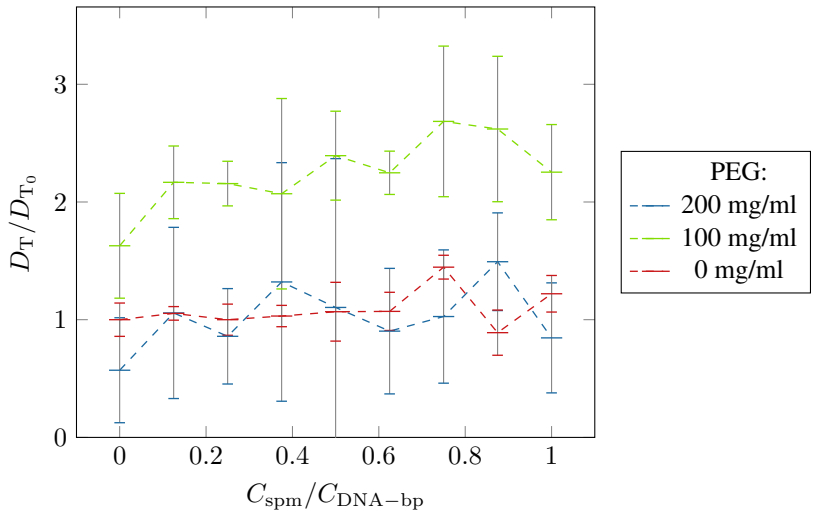

Figure 5.2: Relative change in D_T of complexes in 0 mg/ml, 100 mg/ml and 200 mg/ml PEG, where D_{T_0} is the diffusion constant of the DNA-YOYO-1 complex in the absence of both PEG and spermine. The final DNA concentration is 2 $ng/\mu l$. Lines are guides to the eyes.

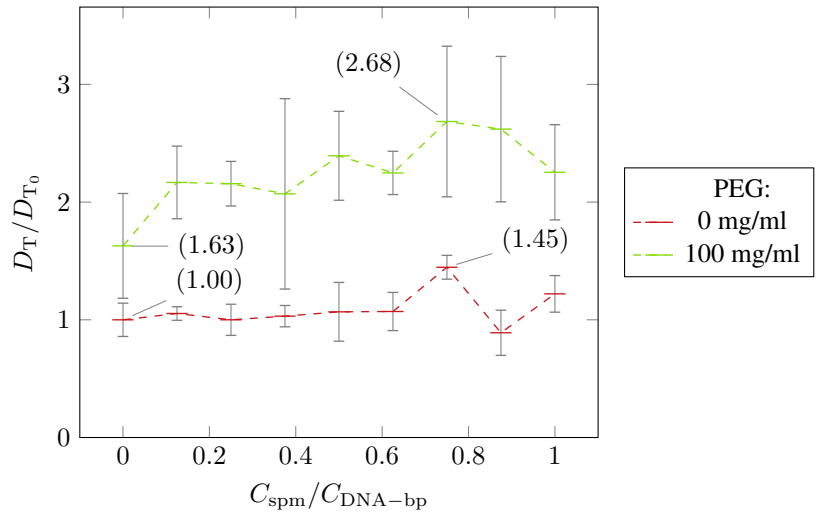

Figure 5.3: Relative change in D_T of complexes in 0 mg/ml and 100 mg/ml PEG, where D_{T_0} is the diffusion constant of the DNA-YOYO-1 complex in the absence of both PEG and spermine. The final DNA concentration is 2 $ng/\mu l$. Lines are guides to the eyes.

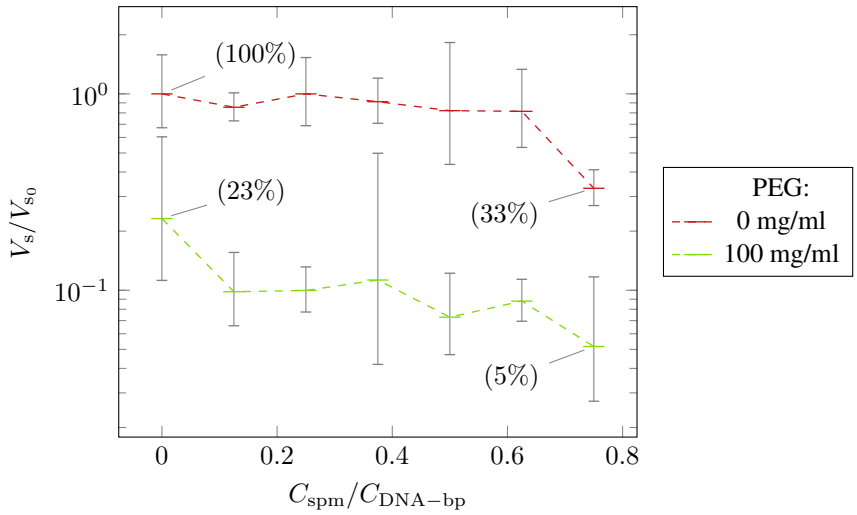

Figure 5.4: Semi-logarithmic plot of the relative change in the assumed spherical hydrodynamic volume, V_s, of complexes in 0 mg/ml and 100 mg/ml PEG. V_{s_0} is the hydrodynamic volume of the DNA-YOYO-1 complex in the absence of both PEG and spermine. The final DNA concentration is 2 $\mathrm{ng}/\mu\mathrm{l}$. Lines are guides to the eyes.

interactions in play which enable GelStar to associate to DNA or to emit more light. The expulsion of the dye seemingly requires a higher level of compaction or precipitation of the DNA.

5.2 New Results

5.2.1 Dye Exclusion by H-NS

The dye exclusion experiments with H-NS were highly inconclusive as little activity was observed. However, as seen in the AFM images in Figure 4.13, there are free stretches of DNA even upon aggregation of H-NS-DNA complexes. This, in addition to a low net condensation as further discussed in Section 5.2.4 could point to a lower amount of actual collapse than what was observed with spermine. This could be appointed to the biological role of H-NS; even though some DNA segments are silenced for expression, and the DNA is somewhat compact, genes still have to be mostly accessible, hence a total collapse is undesirable.

5.2.2 DNA Condensation by PEG and BSA

PEG

The change in diffusion upon addition of PEG is shown as initial values in Figure 4.16, also shown separately in Figure 4.2. Applying viscosity data from Table 4.2 yields the data shown in Figure 5.5. The first conclusion to take from this is that the change in diffusion, and hence the hydrodynamic radius, is little to none. These results of course depend on the viscosity measurements, which could yield error. In the old data, significant condensation was seen at 10% PEG, so one could have expected to see a steady increase in the span 0-6%. This result could be explained by two main differences from the old system, firstly, the old system did not include the addition of $MgCl_2$ to increase H-NS binding. The addition of divalent ions is known to condense DNA, and therefore, PEG may in this case induce less additional condensation, but this can work both ways. Secondly, the 4017 bp PCR product is not as long as the 6010 bp pSB-M2g-1-17 plasmid, which could also affect the relative compaction. Intuition states that the shorter fragment will yield a lower relative compaction, as the limit in the short end would be a rod-like molecule, while a longer polymer would have a superior ability to curl up.

BSA

Little can be concluded about the condensation due to BSA alone, as reliable viscosity data was not obtainable with the methods utilized in this work. What can be noted, is the similarity to PEG when it comes to reduction in diffusion per mass percentage. One could suspect that PEG as a less dense polymer would yield a significantly higher viscosity than BSA, which could be compared to a hard-sphere viscosity estimation model [89].

5.2.3 DNA Condensation by H-NS

Luckily, in the investigations of H-NS activity by FCS, a lower error was achieved than was the case with the previous results with spermine. This is likely the case because this measurement procedure and sample preparation was further optimized, mainly by using silicone isolators to inhibit evaporation, and using covalently stained DNA to minimize interference from rogue dye. The condensation of DNA by H-NS was shown to depend

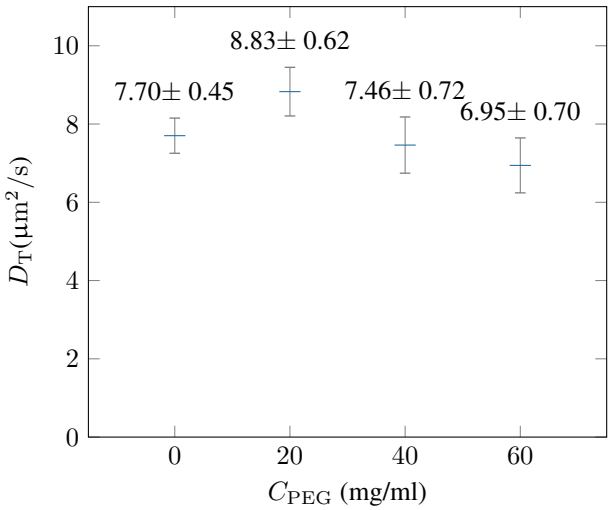

Figure 5.5: Diffusion coefficient D_{T} of 4017 bp PCR product complexes with varying PEG concentration.

highly on the concentration of crowding agents. Compaction by H-NS alone seemed to be variable from set to set, if any compaction could be spotted at all. The amount of condensation visible in Figure 4.15 without PEG was generally not observed in other sets, like in Figure 4.16. This small increase could be due to differences between protein stock aliquots and small changes in temperature, as this affects the binding activity of the protein [90]. The general case seems to be that the error bars increase upon addition of H-NS, but no significant condensation is spotted, which could be explained by the increase in persistence length previously reported in force measurement experiments [90]. So two or perhaps three main competing effects are in play, one is the bridging and bending of DNA by protein, which would lower the hydrodynamic radius and hence, increase diffusion. The second is the stiffening of the DNA polymer when H-NS binds, and thirdly, the volume of the bound protein could be significant, which could also lead to an increase in hydrodynamic radius.

5.2.4 Combined DNA Condensation by PEG and H-NS

In contrast, adding 4% PEG to the H-NS-DNA complexes seems to aid very well in compaction, with a similar result for 6% PEG, also shown in Figure 4.15 and 4.16. Three main effects could be contributing to this. Firstly, as previously mentioned, the protein binds preferably to curved regions of DNA, thus the presumed initial compaction by the crowding agent could induce binding activity. Secondly, the initial bending could allow bridging to happen over longer segments of DNA, structuring it in a more compact overall conformation. Thirdly, the higher viscosity of the solution could stabilize the binding to DNA, as the dispersive thermodynamic forces will experience more resistance in dissociating the protein. This is a similar effect to what one could expect from decreasing the temperature,

as they both lower the diffusion according to Equation 2.1, and some reduction in temperature has been shown to increase binding of H-NS [90]. As previously mentioned, H-NS could be increasing persistence length, but as long as the DNA still compacts enough to get distant segments in proximity to each other, this could be stabilizing the structure in a more compact conformation. If the viscosities from Table 4.2 are taken into account, and we normalize the data to the inital diffusion of DNA at 0% PEG and 0 μM H-NS, we get the numbers in Table 5.1. To get a perhaps more intuitive representation, the data are plotted without the error bars and aggregation points in Figure 5.6.

Table 5.1: Heat map of the viscosity-corrected diffusion coefficients of 4017 bp PCR product under the influence of PEG and H-NS. Red color indicates that aggregation was visible.

	0% PEG	2% PEG	4% PEG	6% PEG
H-NS (μM)	D_T/D_{T_0}			
0.000	1.00±0.06	1.15±0.08	0.97±0.09	0.90±0.09
0.063	1.00±0.06	1.09±0.13	1.15±0.09	0.91±0.07
0.125	1.03±0.10	1.12±0.09	1.08±0.14	1.20±0.07
0.250	0.96±0.07	1.23±0.17	1.16±0.11	1.36±0.09
0.500	1.02±0.07	1.23±0.04	1.40±0.07	0.89±0.24
0.750	1.05±0.11	1.26±0.24	1.24±0.16	-
1.000	1.01±0.09	1.29±0.13	-	-
1.500	0.99±0.12	1.29±0.14	-	-
2.000	0.97±0.17	1.28±0.19	-	-

By calculating the volumetric change of the DNA-complexes under the addition of H-NS, according to Equation 2.5, we get the results in Table 5.2. Here we see that the highest compaction in absence of PEG is 88±19% at 250 nM H-NS, not a very significant result, as the errors span the initial volume. When in a crowded environment on the other hand, 2% PEG yields 46±17% at 1.5 μM, 4% PEG yields 36±9% at 500 nM, and 6% PEG 39±11% at only 250 nM, a very clear pattern showing PEG as an efficient contributor.

5.2.5 Combined DNA Condensation by BSA and H-NS

As no viscosity data was obtained on BSA solutions, it is not possible to say anything certain about initial compaction of the DNA in the absence of H-NS. However, assuming the hydrodynamic radius of the DNA strands to be equal in both 2.5% and 5% BSA, as was approximate in the case with PEG, we could scale the inital values to unity, and see how the addition of H-NS affects the system, as shown in Figure 5.7. In this figure, only the initial increase in diffusion is taken into account, and the points of aggregation were excluded. The maximum change in diffusion here is clearly the higher BSA concentration, at a 136±8% of original diffusion coefficient, which translates to a volume of 40±10% of the original size. This is comparable to the effect of 4 and 6% PEG. In comparison, the 2.5% BSA only led to a volumetric reduction to 85±17% of initial size. An overview of

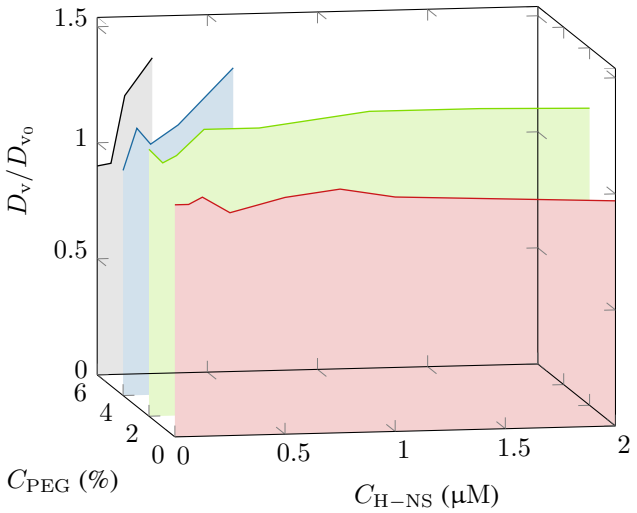

Figure 5.6: Relative viscosity-corrected diffusion coefficients D_v/D_{v_0} as dependent on PEG and H-NS-concentrations.

Table 5.2: Heat map of the relative volumetric changes of 4017 bp PCR product under the influence of PEG and H-NS. Red color indicates that aggregation was visible.

	0% PEG	2% PEG	4% PEG	6% PEG
H-NS (µM)	V_s/V_{s_0}			
0.000	1.00±0.17	0.66±0.18	1.1±0.37	1.37±0.48
0.063	1.01±0.17	0.78±0.32	0.65±0.19	1.33±0.39
0.125	1.09±0.31	0.71±0.2	0.79±0.34	0.57±0.15
0.250	0.88±0.19	0.54±0.24	0.63±0.22	0.39±0.11
0.500	1.06±0.21	0.53±0.11	0.36±0.09	1.43±1.17
0.750	1.14±0.36	0.5±0.3	0.53±0.22	-
1.000	1.02±0.27	0.47±0.17	-	-
1.500	0.98±0.37	0.46±0.17	-	-
2.000	0.91±0.47	0.48±0.24	-	-

the maximum reductions in volume for the crowding conditions in Figure 5.6 and 5.7 are shown in Table 5.3.

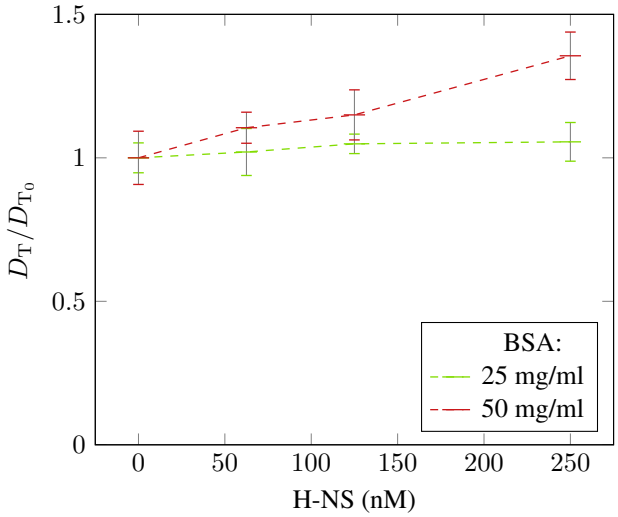

Figure 5.7: Relative change in diffusion coefficient of 2.25 $\mathrm{ng}/\mu\mathrm{l}$ 4017 bp PCR product at different concentrations of H-NS and BSA. Initial diffusion constants are assumed to be similar in both concentrations. Lines are guides to the eyes.

Table 5.3: Maximum volumetric reduction of DNA complexes for given crowding conditions.

Crowding	V_s/V_{s_0}	C_{H-NS} (μM)
0% PEG	88 ± 19%	0.250
2% PEG	46 ± 17%	1.500
4% PEG	36 ± 9%	0.500
6% PEG	39 ± 11%	0.250
2.5% BSA	85 ± 17%	0.250
5.0% BSA	40 ± 10%	0.250

5.2.6 Effect of PEG and H-NS on Expression

After witnessing the joint effects of PEG and H-NS in FCS, some synergism was also expected in the expression assays, but the results shown in Table 4.3 stands inconclusive, or seemingly contrary to this hypothesis. But keeping in mind that the most striking synergism in FCS was observed at 4 and 6% PEG, and that the expression is mostly inhibited already at 4% PEG, it is hard to tell whether or not this challenges the hypothesis. Another important consideration is that while crowding could make the protein bind more easily, and make the traveling distance for particles longer through the solution, it could

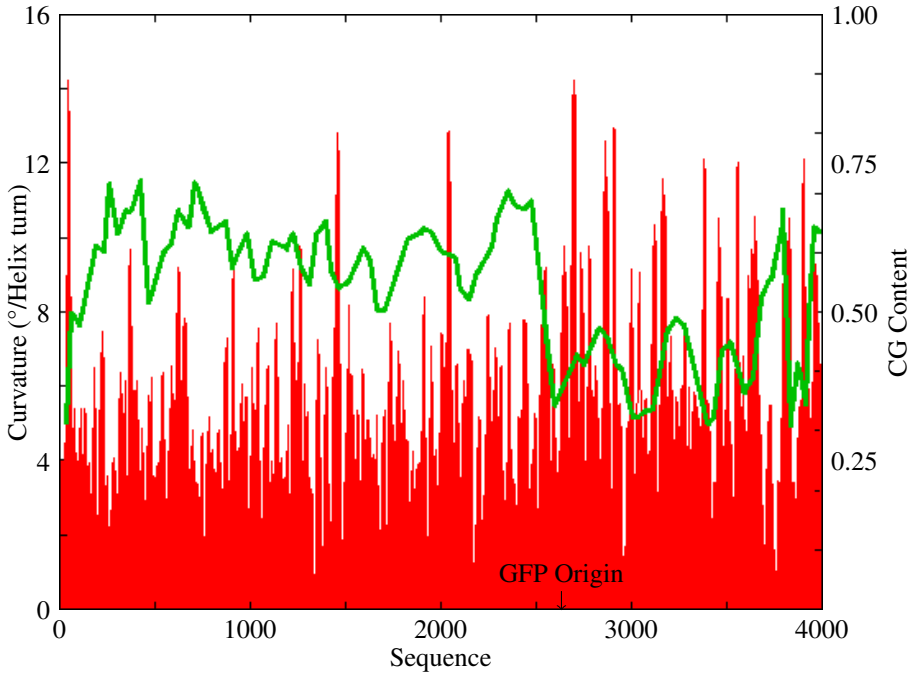

Figure 5.8: The CG content and predicted DNA curvature of 4017 bp PCR product sequence, based on trinucleotide bendability parameters and DNAse I consensus data. CG content is shown as the green line and relates to the right axis labels, while curvature is shown in red columns, corresponding to left axis labels. The T7-promoter starts at base 2528, and the GFP gene starts at base 2634. Acquired by using Bend.it® online software [93]. Apologies for poor resolution, data export was not available.

also localize DNA in more dense regions, as shown in Figure 4.8. This could make the distance shorter for e.g. RNA polymerase, from its termination to a new transcription cycle, and judging by the introductory illustration in Figure 2.4, some effect like this might actually contribute to increased expression. Indicative results for this theory are visible in the column of 2% PEG in Table 4.3. Furthermore, H-NS is known to effectively silence GFP production [91], and this could be due to the aforementioned affinity to AT-rich curved regions. For instance, binding to the TATAAT-box could reduce expression, as it is a transcription promoter sequence found in bacteria [92]. A plot of the GC content and predicted curvature of our DNA using Bend.it® online curvature software [93] is shown in Figure 5.8, and it clearly shows that the GFP gene, following the T7 promoter at base 2528, consists of a region with higher lower CG-content and higher amounts of predicted curvature. This could mean that binding of protein is denser in this region, and silencing is more apparent than compaction as measured by FCS.

5.2.7 AFM Micrographs

The micropgraphs in Figure 4.13 reveal two things in particular. The aggregation is apparent, but free tails of DNA could point to that there is little looping or long-range protein bridging. As the protein binds to the AT-rich regions, it could be that the system is prone to aggregation, since the AT-rich coding part of the amplicon is only approximately a third of the fragment length as shown in Figure 5.8, which means less compaction of single DNA-molecules before separate strands aggregate together. Furthermore, if the regions that H-NS bind more efficiently are already curved, they will be more compact in the first place, making compaction by H-NS even less remarkable. In the micrographs, the coding regions could be the ends of the DNA anchored to the protein oligomers, with the noncoding strands floating more freely.

5.2.8 Electrophoresis Mobility Shift Assays

If little activity would be visible in the binding assays, it would be clearer that an increased amount of bridging was at least partially responsible for the observed increase in diffusion. However, Figure 4.18 through 4.20 shows that the binding is increased, which leaves the long-range bridging mostly inconclusive. Judging from this and the AFM imaging, it seems the protein binds well, but does not necessarily bridge over longer distances.

5.2.9 Notes on Viscosity Correction

The viscosity adjustment was based on the change in diffusion of R6G, which is a small molecule $\simeq$ 1 nm [94][95]. When it comes to this size range, the viscosity of a PEG solution could differ significantly for bodies of different sizes [45]. However, the PEG used in this study is of molecular weight 3,000 Da, and it has been shown that for PEG of this size range, the difference between micro- and macroviscosity is sufficiently low to make this a reasonable estimate [45]. Furthermore, the viscosity experienced by the DNA complexes would be closer to the macroviscosity of the medium than what R6G does, which means that the real increase in translational diffusion would not be lower than this estimate. In any case, R6G is prone to aggregation, and although the standard deviations of these measurements are not too high, they should be considered as rough estimates.

Chapter 6

Conclusion

Although powerful, FCS is a tool very sensitive to aggregation and polydispersity, and requires a high degree of patience and optimization to give good results with DNA. As a single-molecule tool, it requires very finely tuned concentration spans in comparison to FS. From the FCS and EMSA data, it is evident that H-NS both binds and compacts DNA more efficiently in an environment crowded by either BSA or PEG. Observations in AFM and expression assays could be explained by H-NS preferably binding to AT-rich regions, common in transcription promoters, pointing to the protein's role in DNA regulation. In this case, the limit of compaction could be dictated by the AT-density of the DNA fragment, which allows for increased binding affinity, but lower potential reduction in size, due to the intrinsic curvature. H-NS, therefore, can not compete with a nonspecific condensing agent such as spermine when it comes to maximum DNA compaction, but total collapse would in any case be inconvenient in vivo.

Still, it is not clear whether crowding helps compaction due to increased DNA-protein binding, or by any conformational effects. Two experiments could be used to gain clarity in this by using the same FCS setup: First synthesize two sizable ($\geq$2 kbp) amplicons, one of high and one of low AT-content. Then measuring diffusion increase of these upon addition of H-NS and crowding, which could reveal the limits of compaction in each case. By doing the same experiment only with very short fragments ($\sim$12-20 bp), one would expect to see reduction in diffusion coefficients when H-NS binds, as this would increase the hydrodynamic radius of the complex. This could reveal how the binding affinity vs. the compaction is affected by AT-content. Furthermore, an investigation on protein binding in viscous solutions without big macromolecules would help distinguish viscosity effects from volume exclusion effects.

References

[1] Wang GG, Allis CD, Chi P. Chromatin remodeling and cancer, Part II: ATP-dependent chromatin remodeling. *Trends Mol Med,* 2007, 13(9):363-372.

[2] Bloomfield VA. DNA condensation *Curr. Opin. Struct. Biol,* ,1996, 6:334-341.

[3] Teif VB, Lando DY. DNA Condensation Caused by Ligand Binding May Serve as a Sensor. *Sensor Technology,* 2001, p155-160.

[4] Crick, F. Central dogma of molecular biology. *Nature,* 1970, 227:561-563.

[5] Dorman CJ, Nucleoid-associated proteins and bacterial physiology. *Adv. Appl. Microbiol,* 2009, 67:47-64.

[6] Luijsterburg MS, White MF, van Driel R, Dame RT. The major architects of chromatin: architectural proteins in bacteria, archaea and eukaryotes. *Crit Rev Biochem Mol Biol,* 2008, 43:393-418.

[7] Teif VB, Bohinc K. Condensed DNA: Condensing the concepts. *Progress in Biophysics and Molecular Biology,* 2011, 105(3):208-222.

[8] Friedmann T, Roblin R. Gene therapy for human genetic disease? *Science,* 1972, 175:949-955.

[9] Bennett J, Ashtari M, Wellman J, Marshall KA, Cyckowski LL, Chung DC, McCague S, Pierce EA, Chen Y, Bennicelli JL, Zhu X, Ying G-s,Sun J, Wright JF, Auricchio A, Simonelli F, Shindler KS, Mingozzi F, High KA, Maguire AM. AAV2 Gene Therapy Readministration in Three Adults with Congenital Blindness. *Sci Transl Med,* 2012, 4:120ra15.

[10] Sutton A. A Case Against Germ-Line Gene Therapy *Ethics & Medicine,* 2013 29(1):17-22.

[11] Wirth T, Parker N, Yl-Herttuala S. History of gene therapy. *Gene,* 2013, 525(2):162-169.

[12] Bangel-Ruland N,Tomczak K, Fernndez EF, Leier G, Leciejewski B, Rudolph C, Rosenecker J, Weber WM. Cystic fibrosis transmembrane conductance regulator-mRNA delivery: a novel alternative for cystic fibrosis gene therapy. *The journal of gene medicine,* 2013, p414-426.

[13] 2012 Ongoing Clinical trial: β-Thalassemia Major With Autologous CD34+ Hematopoietic Progenitor Cells Transduced With TNS9.3.55 a Lentiviral Vector Encoding the Normal Human β-Globin Gene. `http://clinicaltrials.gov/ct2/show/NCT01639690`

[14] Herweijer H, Wolff JA. Progress and prospects: naked DNA gene transfer and therapy Gene Therapy. *Gene Therapy,* 2003, 10:453-458.

[15] Vannucci L, Lai M, Chiuppesi F, Ceccherini-Nelli L, Pistello M. Viral vectors: a look back and ahead on gene transfer technology. *New Microbiol,* 2013, 36(1):1-22.

[16] Lieleg O, Baumgartel R, M, Bausch AR. Selective Filtering of Particles by the Extracellular Matrix: An Electrostatic Bandpass. *Biophys J,* 2009, 97:1569-1577.

[17] Brinkers S, Dietrich HRC, Groote FHD, Young IT, Rieger B. The persistence length of double stranded DNA determined using dark field tethered particle motion *J Chem Phys,* 2009, 130:p.215105.

[18] Chi Q, Wang G, Jiang J. The persistence length and length per base of single-stranded DNA obtained from fluorescence correlation spectroscopy measurements using mean field theory. *Phys A Stat Mech Appl,* 2012, 392:1072-1079.
[19] Estevez-Torres A, Baigl D. DNA compaction: fundamentals and applications. *Soft Matter,* 2011, 7.15:6746-6756.
[20] Bloomfield VA. Condensation of DNA by multivalent cations: considerations on mechanism. *Biopolymers,* 1991, 31(13):1471-1481.
[21] Chattoraj DK, LC Gosule, JA Schellman. DNA condensation with polyamines. II. Electron microscopic studies. *J Mol Biol,* 1978, 121:327-337.
[22] Olle H. Putrescine, Spermidine, and Spermine *Physiology,* 1986, 1(1)12-15.
[23] Herbst EJ, Snell EE. Putrescine as a growth factor for Hemophilus parainfluenzae. *J Biol Chem,* 1948 176(2):989.
[24] Image from Sigma-Aldrich' online catalogue, cat.# 85590. `http://www.sigmaaldrich.com/catalog/product/sigma/85590`
[25] Flock S, Labarbe R, Houssier C. Dielectric constant and ionic strength effects on DNA precipitation. *Biophysical Journal,* 1996, 70(3):1456-1465.
[26] Liu Y, Chen H, Kenney LJ, Yan J. A divalent switch drives H-NS/DNA-binding conformations between stiffening and bridging modes. *Genes & Dev,* 2010, 24: 339-344.
[27] Effects of pH on Oxaliplatin-Induced Condensation of Single DNA Molecules. Z Hong-Yan, J Chao, L Yu-Ru, L Wei, L Hui, D Shuo-Xing, W Wei-Chi, Z Ling-Yun, X Ping, W Peng-Ye. *Chinese Physics Letters,* 2014, 31(2):28701.
[28] Collapse of DNA Caused by Trivalent Cations: pH and Ionic Specificity Effects. TJ Thomas, VA Bloomfield. *Biopolymers,* 1983, 22:1097-1106.
[29] Plum GE, Arscott PG, Bloomfield VA. Condensation of DNA by trivalent cations. 2. Effect of cation structure. *Biopolymers,* 1990, 30:631-643.
[30] de Coulomb CA. Premier mmoire sur llectricit et le magntisme. *Histoire de lAcadmie Royale des Sciences*, 1785, p.569-577.
[31] Chandra A. Static dielectric constant of aqueous electrolyte solutions: Is there any dynamic contribution? *J Chem Phys,* 2000, 113:903-905.
[32] Zasetsky AY, Svishchev IM. Dielectric response of concentrated NaCl aqueous solutions: Molecular dynamics simulations. *J Chem Phys,* 2001, 115:14481454.
[33] Boresch S, Willensdorfer M, Steinhauser O. A molecular dynamics study of the dielectric properties of aqueous solutions of alanine and alanine dipeptide. *J Chem Phys,* 2004, 120:3333-3347.
[34] Baigl D, Yoshikawa K. Dielectric control of counterion-induced single-chain folding transition of DNA. *Biophys J,* 2005, 88:3486-3493.
[35] Wanichapichart P, Bunthawin S, Kaewpaiboon A, Kanchanapoom K. Determination of cell dielectric properties using dielectrophoretic technique. *ScienceAsia,* 2002, 28:113-119.
[36] Robertson RM, Laib S, Smith DE. Diffusion of isolated DNA molecules: dependence on length and topology. *Proceedings of the National Academy of Sciences,* 2006, 103(19):7310-7314.
[37] Smyth CP, Lundback T, Renzoni D, Siligardi G, Beavil R, Layton M, Sidebotham

JM, Hinton JC, Driscoll PC, Higgins CF, et al Oligomerization of the chromatin-structuring protein H-NS. *Mol Microbiol,* 2000, 36:962-972.

[38] Atlung T, Ingmer H. H-NS: a modulator of environmentally regulated gene expression. *Mol Microbiol,* 1997, 24(1):7-17.

[39] Bloch V, Yang YS, Margeat E, Chavanieu A, Auge MT, Robert B, Arold S, Rimsky S, Kochoyan M. The H-NS dimerization domain defines a new fold contributing to DNA recognition. *Nat Struct Biol* 2003, 10:212-218.

[40] Esposito D, Petrovic A, Harris R, Ono S, Eccleston JF, Mbabaali A, Haq I, Higgins CF, Hinton JC, Driscoll PC, et al. H-NS oligomerization domain structure reveals the mechanism for high order self-association of the intact protein. *J Mol Biol,* 2000, 324:841-850.

[41] Gordon BRG, Li Y, Cote A, Weirauch MT, Ding P, Hughes TR, Navarre WW, Xia B, and Liu J. Structural basis for recognition of AT-rich DNA by unrelated xenogeneic silencing proteins *PNAS* 2011, 108(26):10690-10695.

[42] Navarre WW, Porwollik S, Wang Y, McClelland M, Rosen H, Libby SJ, Fang FC. Selective silencing of foreign DNA with low GC content by the H-NS protein in Salmonella. *Science,* 2006, 313:236-238.

[43] Image generated with JavaScript PV (Protein Viewer) using X-ray diffraction structure data from RCSB Protein Data Bank (DOI:10.2210/pdb3nr7/pdb). Primary structure source: Arold ST, Leonard PG, Parkinson GN, Ladbury JE. H-NS forms a superhelical protein scaffold for DNA condensation. *Proc. Natl. Acad. Sci. USA,* 2010, 107:15728-15732.

[44] Image generated with JavaScript PV (Protein Viewer) using NMR data from RCSB Protein Data Bank (DOI:10.2210/pdb2lev/pdb). Primary structure source: Cordeiro TN, Schmidt H, Madrid C, Juarez A, Bernado P, Griesinger C, Garcia J, Pons M. Indirect DNA readout by an H-NS related protein: structure of the DNA complex of the C-terminal domain of Ler. *Plos Pathog,* 2011, 7:e1002380-e1002380.

[45] Holyst R, Bielejewska A, Szymanski J, Patkowski A, Gapinski J,Zywocinski A, Kalwarczyk T, Kalwarczyk E, Tabaka M, Natalia Ziebacz N, Wieczoreka SA. Scaling form of viscosity at all length-scales in poly(ethylene glycol) solutions studied by fluorescence correlation spectroscopy and capillary electrophoresis. *Physical Chemistry Chemical Physics*. 2009, 11.40:9025-9032.

[46] Cha S, Kim SH, Kim D. Viscosity of Sucrose Aqueous Solutions Measured by Using Fluorescence Correlation Spectroscopy. *Journal of the Korean Physical Society,* 2010, 56(4):1315-1318.

[47] Illustration by David S. Goodsell, the Scripps Research Institute. `http://mgl.scripps.edu/people/goodsell/illustration/public/ecoli.tif` - Fetched June 5th 2015.

[48] Miyoshi D, Sugimoto N. Molecular crowding effects on structure and stability of DNA. *Biochimie,* 2008, 90(7):1040-1051.

[49] Linegar KL, Adeniran AE, Kostko AF, Anisimov MA. Hydrodynamic Radius of Polyethylene Glycol in Solution Obtained by Dynamic Light Scattering. *Colloid Journal,* 2010, 72(2):279-281.

[50] Axelsson I. Characterization of Proteins and Other Macromolecules by agarose Gel Chromatography. *Journal of Chromatography,* 1978, 152:21-32.

[51] Image courtesy of MP Biomedicals online catalogue, cat.# 02194839. http://www.mpbio.com/product.php?pid=02194839
[52] Böhme U, Scheler U. Effective charge of bovine serum albumin determined by electrophoresis NMR. *Chemical Physics Letters,* 2007, 435:342-345.
[53] Zimmerman SB, Minton AP. Macromolecular Crowding: Biochemical, Biophysical, and Physiological Consequences. *Annu. Rev. Biaphys. Biamal. Struct,* 1993, 22:27-65.
[54] Tan L, Liu L, Xie Q, Zhang Y, Yao S. Fluorescence quenching of bovine serum albumin. *Anal Sci,* 2004, 20(3):441-444.
[55] Ryder SP, Recht MI, Williamson JR. Quantitative analysis of protein-RNA interactions by gel mobility shift. *Methods in molecular biology,* 2008, 488:99-115.
[56] Hellman LM, Fried MG. Electrophoretic Mobility Shift Assay (EMSA) for Detecting Protein-Nucleic Acid Interactions. *Nature protocols,* 2007, 2(8):1849-1861.
[57] Image generated with JavaScript PV (Protein Viewer) using X-ray diffraction structure data from RCSB Protein Data Bank (DOI:10.2210/pdb4or0/pdb). Primary structure source: Bujacz A, Zielinski K, Sekula B. Structural studies of bovine, equine, and leporine serum albumin complexes with naproxen. *Proteins,* 2014, 82:2199-2208.
[58] Gonzalez-Tello P, Camacho F, Blazquez G. Density and Viscosity of Concentrated Aqueous Solutions of Polyethylene Glycol. *J Chem Eng Data,* 1994, 39:611-614.
[59] Harvard University - Department of Physics: A Summary of Error Propagation. http://ipl.physics.harvard.edu/wp-uploads/2013/03/PS3_Error_Propagation_sp13.pdf - Fetched June 3rd 2015.
[60] Life Technologies - DNA and RNA Molecular Weights and Conversions. https://www.lifetechnologies.com/no/en/home/references/ambion-tech-support/rna-tools-and-calculators/dna-and-rna-molecular-weights-and-conversions.html - Fetched June 4th 2015.
[61] Dame RT, Wyman C, Goosen N. H-NS mediated compaction of DNA visualised by atomic force microscopy *Nucleic Acids Res,* 2000, 28(18):3504-3510.
[62] Luczka J, Talkner P, Hanggi P. Diffusion of Brownian particles governed by fluctuating friction. *Physica A,* 2000, 278:18-31.
[63] Fischer H, Polikarpov I, Craievich AF. Average protein density is a molecular-weight-dependent function. *Protein Sci,* 2004, 13(10):28252828.
[64] Schildkraut CL, Marmur J, Doty P. Determination of the base composition of deoxyribonucleic acid from its buoyant density in CsCl. *J Mol Biol,* 1962, 4:430-443.
[65] McLennan JA. Introduction to Nonequilibrium Statistical Mechanics, 1989, Prentice-Hall, Englewood Clis, NJ. p.54.
[66] Promega - Protocols & Applications Guide - Chapter 5 https://no.promega.com/~/media/files/resources/paguide/a4/chap5a4.pdf?la=en - Fetched May 4th 2015.
[67] Wong ML, Medrano JF. Real-time PCR for mRNA quantitation. *BioTechniques,* 2005, 39:75-85

[68] Borlinghaus RT. Confocal Optical Section Thickness. *Leica Microsystems* June 21st, 2011. http://www.leica-microsystems.com/science-lab/confocal-optical-section-thickness

[69] Robertson RM, Laib S, Smith DE. Diffusion of isolated DNA molecules: Dependence on length and topology *PNAS,* 2006, 103(19):7310-7314.

[70] PicoQuant Tutorial: Calculate and Fit FCS Traces with the FCS Script (2013), http://www.picoquant.com/images/uploads/downloads/calculate_and_fit_fcs-traces_with_the_fcs-script_step_by_step.pdf - Fetched September 13th 2014.

[71] W Pauli. ber den Zusammenhang des Abschlusses der Elektronengruppen im Atom mit der Komplexstruktur der Spektren. *Z. Phys,* 1925, 31:765.

[72] Enderlein J, Gregor I. Using fluorescence lifetime for discriminating detector afterpulsing in fluorescence-correlation spectroscopy. *Rev Sci Insrum,* 2005, 76(3):033102-033102-5.

[73] Zhao M, Jin L, Chen B, Ding Y, Ma H, Chen D. Afterpulsing and its correction in fluorescence correlation spectroscopy experiments. *Appl Optics,* 2003, 42(19):4031-4036.

[74] Efron B. The jackknife, the bootstrap and other resampling plans. 1980. Division of Biostatistics, Stanford University.

[75] Based on phone call with PicoQuant Support Center 14:02 June 12th 2015. Tel: +49-30-6392-6929. - No literature on the specific bootstrapping algorithm used in Symphotime is officially available.

[76] Laniel M-A, Bliveau A, Gurin SL. Electrophoretic Mobility Shift Assays for the Analysis of DNA-Protein Interactions *Methods in Molecular Biology,* 2001, 148:13-30.

[77] Promega Miniprep Quick Protocol: https://no.promega.com/~/media/files/resources/protcards/wizard%20plus%20sv%20minipreps%20dna%20purification%20system%20quick%20protocol.pdf - Fetched September 12th 2014.

[78] Phenol/Chloroform Extraction and Ethanol Precipitation provided by Thermo Scientific. http://www.thermoscientificbio.com/uploadedFiles/Resources/phenol-chloroform-extraction-ethanol-precipitation.pdf - Fetched September 23rd 2014.

[79] QIAexpress Ni-NTA Fast Start Handbook. file:///home/chronos/u-144bf4086fef0cfa34eeca4fb572eee494d5322a/Downloads/EN-QIAexpress-Ni-NTA-Fast-Start-Handbook.pdf - Fetched August 17th 2015.

[80] Bio-Rad: Quick Start™ Bradford Protein Assay Instruction Manual http://www.bio-rad.com/webroot/web/pdf/lsr/literature/4110065A.pdf - Fetched November 17th 2014.

[81] Vogel R, Meredith P, Harvey MD, Rubinsztein-Dunlop H. Absorption and fluorescence spectroscopy of rhodamine 6G in titanium dioxide nanocomposites.

Spectrochimica Acta, 2004, A60.245249.

[82] HS Rye, S Yue, DE Wemmer, MA Quesada, RP Haugland, RA Mathies, AN Glazer. Stable fluorescent complexes of double-stranded DNA with bis-intercalating asymmetric cyanine dyes: properties and applications. *Nucleic Acids Res,* 1992, 20(11):2803-2812.

[83] TNT® Quick Protocol. Quick Coupled Transcription/Translation Systems `https://no.promega.com/~/media/files/resources/protcards/tntquickcoupledtranscription-translationsystemsquickprotocol.pdf` - Fetched August 20th 2014.

[84] Leica Microsystems - Leica motCORR objectives. `http://www.leica-microsystems.com/fileadmin/downloads/Leica%20TCS%20SP5%20II/Brochures/Leica%20motCorr-Flyer_EN.pdf` - Fetched June 12th 2015.

[85] Picoquant: Absolute Diffusion Coefficients: Compilation of Reference Data for FCS Calibration. `http://www.picoquant.com/images/uploads/page/files/7353/appnote_diffusioncoefficients.pdf` - Fetched October 5th 2014.

[86] Patra S, Santhosh K, Pabbathi A, Samanta A. Diffusion of organic dyes in bovine serum albumin solution studied byfluorescence correlation spectroscopy. *RSC Adv,* 2012, 2:6079-6086

[87] Yadav S, Shire SJ, Kalonia DS. Viscosity Analysis of High Concentration Bovine Serum Albumin Aqueous Solutions. *Pharmaceutical Research,* 2011, 28(8):1973-1983.

[88] Gill DS, Ali V. Behavior of bovine serum albumin in aqueous solutions of some sodium salts of organic acids, tetraethylammonium bromide and dextrose investigated by ultrasonic velocity, viscosity and density measurements. *Indian journal of chemistry,* 1999, 38(7):651-655.

[89] Minton AP. Hard Quasispherical Particle Models for the Viscosity of Solutions of Protein Mixtures. *J Phys Chem B,* 2012, 116(31):9310-9315.

[90] Amit R, Oppenheim AB, Stavans J. Increased bending rigidity of single DNA molecules by H-NS, a temperature and osmolarity sensor. *Biophys J,* 2003, 84(4):2467-2473.

[91] Corcoran CP, Cameron ADS, Dorman CJ. H-NS Silences gfp, the Green Fluorescent Protein Gene: gfpTCD Is a Genetically Remastered gfp Gene with Reduced Susceptibility to H-NS-Mediated Transcription Silencing and with Enhanced Translation. *J. Bacteriol,* 2010, 192(18):4790-4793.

[92] Pribnow D. Nucleotide sequence of an RNA polymerase binding site at an early T7 promoter. *PNAS,* 1975, 72(3):784-788.

[93] `http://hydra.icgeb.trieste.it/dna/bend_it.html`

[94] Penzkofer A, Lu Y. Fluorescence quenching of rhodamine 6G in methanol at high concentration, *Chem Phys,* 1986, 103:399-405.

[95] Penzkofer A, Lu Y. Absorption behaviour of methanolic rhodamine 6G solutions at high concentration. *Chemical Physics,* 1986, 107:175-184.